A numerical comparison of approximations to the Stokes equations used in ice sheet and glacier modeling

R. C. A. Hindmarsh

Physical Science Division, British Antarctic Survey, Cambridge, UK

Received 3 July 2003; revised 8 October 2003; accepted 4 November 2003; published 10 March 2004.

[1] A computational analysis of the accuracy of different approximations to the Stokes equations for momentum balance used in ice sheet modeling is performed by solving a particular tractable form of the equations appropriate for small perturbations of the ice surface, describing the uniform flow of ice with a Glen rheology on an infinitely long and broad section. The approximants comprise the shallow ice approximation and various schemes for incorporating longitudinal stresses and, in one case, the horizontal gradient of the horizontal plane shear stresses. The simplifications lead to a vertically one-dimensional numerical problem, whose solution can be computed rapidly. The relaxation rate of perturbations as well as other response descriptors for the stable full system and approximants are compared. Compared with the shallow ice approximation, the inclusion of longitudinal stresses increases accuracy at shorter wavelengths, but accuracy is poor at wavelengths around or less than the ice sheet thickness. Even though analysis shows that the horizontal gradients of the horizontal plane shear stresses are of similar magnitude to longitudinal stress effects, computations show, in agreement with glaciological belief, that longitudinal stress effects are more significant and need to be corrected for first in practice. Two schemes, a multilayer scheme and a one-layer scheme, are particularly good and should be investigated further in cases where perturbations from uniformity are large. Some other apparently plausible approximations introduce nonphysical instabilities. New schemes need to be assessed in the way described in this paper before being used in real ice sheet models. *INDEX TERMS:* 1827 Hydrology: Glaciology (1863); 3210 Mathematical Geophysics: Modeling; 3230 Mathematical Geophysics: Numerical solutions; *KEYWORDS:* ice sheets, mechanics, mathematical geophysics

Citation: Hindmarsh, R. C. A. (2004), A numerical comparison of approximations to the Stokes equations used in ice sheet and glacier modeling, *J. Geophys. Res.*, *109*, F01012, doi:10.1029/2003JF000065.

1. Introduction

[2] Ice sheet models have hitherto generally used the shallow ice approximation to the Stokes equations, but a recent theme has been the incorporation of further mechanical effects, principally longitudinal stress gradients. (When glaciologists refer to longitudinal stresses, they mean all stress tensor components apart from the two horizontal plane (HP) shear components.) This paper presents a computational analysis of the accuracy of different approximations by comparing solutions of Fourier transforms of linearizations of these approximants to those of the full momentum-balance equations. As compared with solving the full nonlinear equations, the advantage of solving Fourier transforms of the linearized equations, which perforce must deal with small perturbations, is the greatly reduced computational effort and the certainty that horizontal discretization effects are not contaminating the results. These analyses of linearized equations give a definitive result regarding Stokes equations approximants; if they are not good for small perturbations, they are useless.

[3] The approximants all in some way start from the shallow ice approximation (SIA [*Hutter*, 1983]) and, like this approximation, involve dropping terms from the momentum balance equations and simplifying the strain rate definitions. However, the approximants contain more terms than the SIA under the supposition that this decreases the error of the approximation. This paper investigates this assumption. The SIA is a development of earlier shallow theories [e.g., *Nye*, 1959] but significantly extends their usefulness by giving explicit error estimates. Work in the early 1980s [*Hutter*, 1983; *Morland*, 1984] showed that the SIA was an asymptotic expansion of the Stokes equations in terms of the aspect ratio (height/span ratio), denoted δ in this paper. The SIA is accurate to $O(\delta^2)$. The SIA shows clearly that for lubrication flows where sliding is small the vertical gradient of the horizontal plane shear stresses balances the pressure

0148-0227/04/2003JF000065$09.00

gradients and that the neglected terms (horizontal gradients of all stress components) both contribute error at second order in the relevant expansion parameter. The SIA actually states that for no slip the inclusion of longitudinal stress effects does not improve accuracy unless one simultaneously considers the horizontal gradients of the HP shear stresses. However, it is generally considered by glaciologists that one needs to model longitudinal stress gradients first [*Robin*, 1967; *Collins*, 1968; *Nye*, 1969; *Budd*, 1970; *Kamb and Echelmeyer*, 1986; *Dahl-Jensen*, 1989; *Van der Veen and Whillans*, 1989; *Blatter*, 1995].

[4] A confounding factor is that the accuracy of the SIA decreases as the amount of basal slip increases [*Gudmundsson*, 2003]. The shallow theory for ice shelf spreading, where the proportion of slip is very high, balances the vertical gradient of the HP shear stresses with the horizontal gradients of the longitudinal stresses as well as the pressure gradient, and it is widely acknowledged that these gradients must play a role in well-lubricated grounded stream flows [*Muszynski and Birchfield*, 1987; *MacAyeal*, 1989]. Further analysis requires the introduction of one of two equivalent parameters, the traction number (ratio of basal tangential traction to surface stress deviator [*Hindmarsh*, 1993]) or the slip ratio (the ratio of the sliding velocity to the difference between surface and basal velocity). *Hindmarsh* [1993] and *Wilchinsky and Chugonov* [2000] have shown how the approximation error depends on the degree of slip, and they also show that a shallow long-wavelength theory suffices for all possible slip ratios. R. C. A. Hindmarsh (Mechanics of the sheet-stream-shelf transition, submitted to *Continuum Mechanics and Thermodynamics*, 2004, hereinafter referred to as Hindmarsh, submitted manuscript, 2004) has produced a single-layer scheme that is uniformly accurate at $O(\delta^2)$, formally of the same order of error as the multilayer schemes alluded to above. *Hindmarsh* [1993] also analyzed a simpler scheme, with accuracy dependent on the degree of slip with maximum error $O(\delta)$.

[5] There have been few direct comparisons of the SIA with solutions of the Stokes equations. *Johannesson* [1992] and *Gudmundsson* [2003] both carry out linearized studies of the free surface problem. *Gudmundsson* [2003] focuses on how the slip ratio affects the validity of the SIA. This paper is concerned with these issues but particularly considers how the accuracy of the Stokes equations approximants is affected by the combined effects of slip ratio and wavelength. *Leysinger Vieli and Gudmundsson* [2004] compare solutions of the Stokes equations and the SIA for the flow of a glacier down an inclined plane. At short wavelength, non-SIA effects become important.

[6] The computational advantage of the SIA is that it reduces the computational problem of Stokes flow, which is a three-dimensional problem in four variables (three velocity components and, commonly, the pressure) to a two-dimensional problem in the thickness. *Blatter* [1995] constructed a scaling where the longitudinal stress terms and longitudinal stress gradient terms play a significant role and implemented this in a numerical scheme. Such "longitudinal stress schemes" are used widely in ice sheet modeling [*Huybrechts*, 1992; *Hubbard et al.*, 1998; *Pattyn*, 2003; *Ritz et al.*, 2001; *Saito et al.*, 2004]. Longitudinal stress approximations introduce the two horizontal velocity components as field variables. One therefore has to solve elliptic systems for two rather than for four variables of the full system at points in three-dimensional space [see, e.g., *Pattyn*, 2003, equations (18) and (19)], and the resultant linear systems are generally better conditioned than those resulting from the numerical analysis of the full system. These models are termed "multilayer models." There is also a class of longitudinal stress models that solve an elliptic system at one elevation only (generally the upper surface), and the resulting problem is therefore computationally two-dimensional. Clearly the accuracy of such single-layer schemes will be less than those of multilayer schemes, but it appears from asymptotic analysis that some single-layer schemes may be of comparable accuracy to the multilayer schemes (Hindmarsh, submitted manuscript, 2004) as both are formally $O(\delta^2)$. This paper compares the accuracy of single-layer and multilayer schemes.

[7] The means of comparison of these various schemes with the SIA and the full Stokes equations is as follows. Following *Johannesson* [1992] and *Gudmundsson* [2003], the quasi-uniform Stokes flow of a fluid with a nonlinear rheology on the infinite plane is linearized and Fourier transformed to provide a complex one-dimensional eigenvalue problem in the vertical domain. A similar perturbation procedure can be carried out for approximations to the Stokes equations. The Stokes flow is stable, and the spectrum (i.e., the dependence of the decay constant for perturbations on the wavelengths parallel and transverse to the main flow direction) of this flow can be compared with spectra computed for Stokes flow approximants. Analytical solutions have been obtained for the case of a Newtonian rheology by *Gudmundsson* [2003], who provides an up-to-date review of previous glaciological work in this area. It will be seen that the qualitative features of the spectra for nonlinear fluids follow examples for linear fluids given by *Gudmundsson* [2003], and in particular, the qualitative forms of the spectra he found for flow at high slip ratio are found to also occur for nonlinear rheologies. A similar numerical perturbation for nonlinear rheologies has been carried out by *Johannesson* [1992]. Differences between his study and the present case lie in different formulations of the perturbation problem, different approaches to regularizing the zeroth-order problems, and in the means of solution of the numerical eigenvalue problem. *Johannesson* [1992] combines streamline and stress functions in a finite difference formulation in physical space, while the present paper uses a primitive variable formulation in a mapped space that follows the free surface, with a pseudo-spectral approach to discretization.

[8] The flow of a Glen fluid down the infinite plane leads to an infinite viscosity at the surface owing to the vanishing of the stress. This is not physical, and various schemes for dealing with this have been considered [*Hutter*, 1983; *Johannesson*, 1992; *Baral et al.*, 2001]. In this paper, an assumption of quasi-uniform flow is used. It is assumed that the flow is extending (positive longitudinal strain rate) in the main direction of flow. This establishes a nonzero strain rate and a corresponding deviatoric stress component at the upper surface, which prevents the viscosity from being singular. This strain rate also induces a vertical velocity that

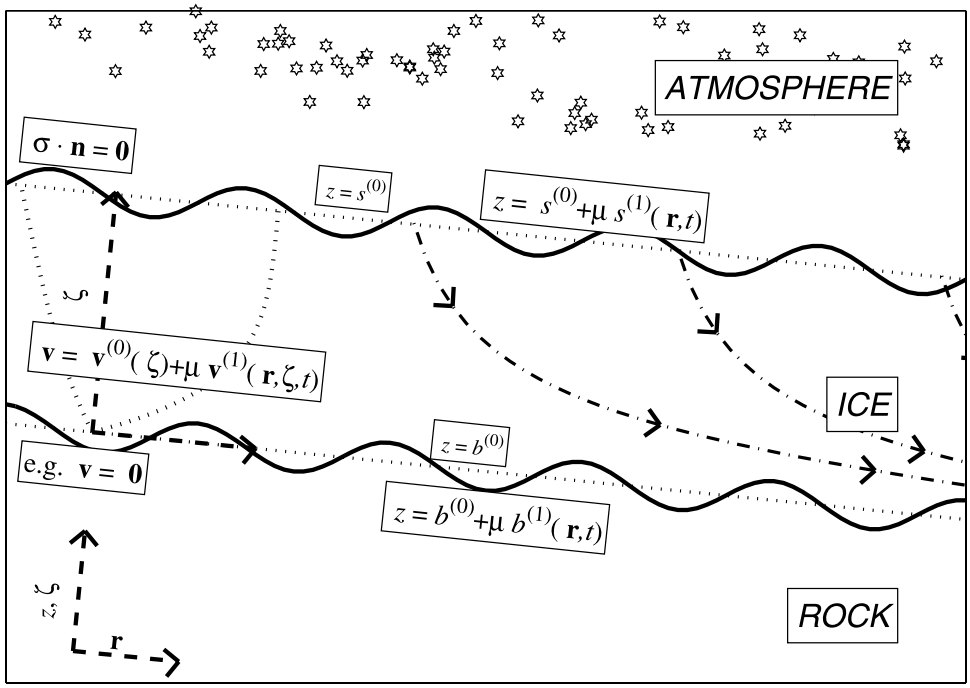

Figure 1. Illustration of the problem setup and coordinate system.

balances an accumulation rate. In a situation where the ice thickness is uniform the input of snow should require the flow to accelerate. The assumption of quasi-uniform flow states that when sufficiently short wavelengths are being considered, the mean flow velocity does not increase substantially over this length scale and can be regarded as constant. The errors associated with this assumption obviously deteriorate as wavelength increases. We shall not be considering this in detail as at long wavelengths the SIA, which does not explicitly need to consider this singularity, holds anyhow.

[9] The paper plan is to present the basic equations for slow isothermal flow, to define several Stokes flows approximants, and to describe how these equations are linearized and their relaxation spectra computed. Comparisons are made as a function of wavelength, slip ratio, and basal physics.

2. Stokes Equations

[10] The setup of flow down an infinite plane is illustrated in Figure 1. Dimensional quantities are represented by a tilde and nondimensional quantities without a tilde. Fourier transforms are represented by a caret. The coordinates are $(\tilde{x}, \tilde{y}, \tilde{z})$, where $\tilde{z}$ is perpendicular to the base plane and $\tilde{x}$ is in the zeroth-order flow direction. The $\tilde{z}$ direction is called "vertical," and the $\tilde{\mathbf{r}} = (\tilde{x}, \tilde{y})$ plane is called "horizontal." The upper and lower surfaces are given by $\tilde{z} = \tilde{s}(\tilde{\mathbf{r}}, \tilde{t})$ and $\tilde{z} = \tilde{b}(\tilde{\mathbf{r}}, \tilde{t})$, respectively, the thickness of the ice is given by $\tilde{H}(\tilde{\mathbf{r}}, \tilde{t}) = \tilde{s}(\tilde{\mathbf{r}}, \tilde{t}) - \tilde{b}(\tilde{\mathbf{r}}, \tilde{t})$, and $\tilde{t}$ represents time. Subscripts (b) and (s) indicate evaluation at the surface or base, respectively. The operators ∇_{H} and $\nabla_{\mathrm{H}}\cdot$ represent the horizontal gradient and divergence, respectively.

[11] The three-dimensional velocity field is conveniently represented by the vertical velocity $\tilde{w}$ and the horizontal velocity vector $\tilde{\mathbf{u}} = (\tilde{u}_x, \tilde{u}_y)$, and we also use $\tilde{\mathbf{v}} = (\tilde{u}_x, \tilde{u}_y, \tilde{w})$. The governing equations, which apply to all $\tilde{\mathbf{r}}$, are

$$\nabla_{\mathrm{H}}\cdot\tilde{\mathbf{u}} + \partial_{\tilde{z}}\tilde{w} = 0, \qquad \tilde{b} \le \tilde{z} \le \tilde{s}, \tag{1}$$

$$\nabla \cdot \tilde{\boldsymbol{\sigma}} + \tilde{\rho}\tilde{\mathbf{g}} = 0, \qquad \tilde{b} \le \tilde{z} \le \tilde{s}, \tag{2}$$

$$\tilde{\boldsymbol{\sigma}}_{(s)} \cdot \mathbf{n}_{(s)} = 0, \qquad \tilde{z} = \tilde{s}, \tag{3}$$

$$\left.\begin{aligned} \mathbf{v}_{(b)} &= 0, \text{ no slip,} \\ \text{equation(6), } \mathbf{n}_{(b)} \cdot \mathbf{v}_{(b)} &= 0, \text{ sliding,} \end{aligned}\right\} \quad \tilde{z} = \tilde{b}. \tag{4}$$

Here, equation (1) expresses conservation of mass in the ice; equations (2), (3), and (4) describe conservation of momentum in the ice, where $\tilde{\boldsymbol{\sigma}}$ is the stress tensor, $\tilde{\rho}$ is the density of ice, $\tilde{\mathbf{g}} = \tilde{g}(\epsilon, 0, -1)$ is the gravitational acceleration vector, and $\mathbf{n}$ is the normal vector at the indicated surface. The horizontal component of gravity $\epsilon\tilde{g}$ is functionally equivalent to a slope of ϵ. The constitutive relations comprise (1) a nonlinear viscous relationship within the ice:

$$\tilde{\mathbf{e}} = \tilde{A}_c|\tilde{\tau}|^{n-1}\tilde{\boldsymbol{\tau}}, \tag{5}$$

where $\tilde{\mathbf{e}}$ is the strain rate tensor, $\tilde{\tau}$ is a second invariant of the deviator stress tensor, $\tilde{\boldsymbol{\tau}}$, n is the Glen index, and $\tilde{A}_c$ is a rate factor; and (2) an isotropic sliding relation of the form

$$\tilde{\mathbf{u}}_{\|(b)} = \tilde{A}_s\left|\tilde{\mathbf{T}}_{t(b)}\right|^{\ell-1}\tilde{\mathbf{T}}_{t(b)}/\tilde{p}_e^{\nu}, \tag{6}$$

where $\tilde{\mathbf{u}}_{\|(b)}$ is the sliding velocity, $\tilde{\mathbf{T}}_{t(b)}$ is the basal tangential traction, ℓ is the sliding index, $\tilde{A}_s$ is the sliding rate factor, $\tilde{p}_e = -\tilde{T}_n - \tilde{p}_w$ is the effective pressure, $\tilde{T}_n$ is the normal traction, $\tilde{p}_w$ is the subglacial water pressure, and ν is a further index.

[12] The assumption of quasi-uniform flow states that such a flow $\tilde{\mathbf{v}}^{(\mathrm{SQU})}$ is given by

$$\tilde{\mathbf{v}}^{(\mathrm{SQU})} = \left(\tilde{v}_{\tilde{x}}^{(\mathrm{SQU})}, 0, \tilde{v}_{\tilde{z}}^{(\mathrm{SQU})}\right), \qquad \tilde{\boldsymbol{\nabla}} \cdot \tilde{\mathbf{v}}^{(\mathrm{SQU})} = 0, \tag{7}$$

where $\tilde{\mathbf{v}}^{(\mathrm{SQU})}$ is treated as being independent of $\tilde{\mathbf{r}}$, but $\partial_{\tilde{x}} \tilde{v}_{\tilde{x}}^{(\mathrm{SQU})}$ may be nonzero. Essentially, it is being assumed that over one wavelength $\partial_{\tilde{x}} \tilde{v}_{\tilde{x}}^{(\mathrm{SQU})}$ is sufficiently small that the $\tilde{\mathbf{r}}$ independence of $\tilde{\mathbf{v}}^{(\mathrm{SQU})}$ is a valid assumption. This assumption is applied to the base flow about which linearization is performed.

3. Stokes Equations Approximants

[13] We now define several Stokes equations approximants. The continuity equation $\tilde{\boldsymbol{\nabla}} \cdot \tilde{\mathbf{v}} = 0$ is satisfied in all the approximations. The assumption of quasi-uniform flow is used in all cases apart from the SIA. The following notation is used:

$$\tilde{\tau}_s^{(\cdot)2} = \tilde{\tau}_{xz}^{(\cdot)2} + \tilde{\tau}_{yz}^{(\cdot)2}, \quad 2\tilde{\tau}_\ell^{(\cdot)2} = \tilde{\tau}_{xx}^{(\cdot)2} + \tilde{\tau}_{yy}^{(\cdot)2} + \tilde{\tau}_{zz}^{(\cdot)2} + 2\tilde{\tau}_{xy}^{(\cdot)2}, \tag{8}$$

$$j = (x, y), \qquad k = (x, y), \tag{9}$$

and the non-HP strain rate components are always defined:

$$e_{jk} = \frac{1}{2}\left(\partial_k \tilde{v}_j + \partial_j \tilde{v}_k\right). \tag{10}$$

The center dot is used as a "wild card" to represent missing letters from items contained in the following set $\mathcal{A}$ = {S, L1S1, L1S2, L1L1, L1L2, LMLa, LMLb, LTSML}, e.g., the center dot represents the whole set, L1· represents {L1S1, L1S2, L1L1, L1L2}, etc. These abbreviations refer to Stokes equations approximants that will be defined in sections 3.1 and 3.2. Superscripts give information about the approximant being used. A superscript in parentheses containing a member of the set $\mathcal{A}$ shows that the superscripted quantity has been computed according to the corresponding approximation scheme.

3.1. Lubrication Theory Approximations

[14] In this class of approximations, vertical HP shear stress gradients are balanced by the pressure gradients and the downstream body force. Thus the field equations are approximated by

$$\left.\begin{aligned} \partial_{\tilde{z}} \tilde{\tau}_{xz}^{(\mathrm{S})} &= \partial_{\tilde{x}} \tilde{p}^{(\mathrm{S})} - \tilde{\rho}\tilde{g}\epsilon, \qquad \partial_{\tilde{z}} \tilde{\tau}_{yz}^{(\mathrm{S})} = \partial_{\tilde{y}} \tilde{p}^{(\mathrm{S})}, \\ -\partial_{\tilde{z}} \tilde{p}^{(\mathrm{S})} &= \tilde{\rho}\tilde{g}, \\ \tilde{\tau}^{(\mathrm{S})2} &= \tilde{\tau}_{xz}^{(\mathrm{S})2} + \tilde{\tau}_{yz}^{(\mathrm{S})2}, \qquad \tilde{e}_{jz}^{(\mathrm{S})} = \tfrac{1}{2}\partial_{\tilde{z}} \tilde{u}_j^{(\mathrm{S})}. \end{aligned}\right\} \tag{11}$$

where $\tilde{p}$ is the pressure, with boundary tractions given by

$$\left.\begin{aligned} \tilde{\tau}_{jz(s)}^{(\mathrm{S})} &= 0, \qquad & \tilde{\sigma}_{zz(s)}^{(\mathrm{S})} &= 0, \\ \tilde{\tau}_{jz(b)}^{(\mathrm{S})} &= \tilde{T}_{tj(b)}^{(\mathrm{S})}, \qquad & \tilde{\sigma}_{zz(b)}^{(\mathrm{S})} &= -\tilde{p}^{(\mathrm{S})}. \end{aligned}\right\} \tag{12}$$

3.1.1. (S): Shallow Ice Approximations

[15] This is the standard shallow ice approximation (11) and (12).

3.1.2. (SQU): Shallow Ice Approximation With Quasi-Uniform Flow

[16] This is as the shallow ice approximation, except

$$\tilde{\tau}^{(\mathrm{SQU})2} = \tau_s^{(\mathrm{SQU})2} + \tau_\ell^{(\mathrm{SQU})2}. \tag{13}$$

3.2. Longitudinal Stress Approximations

[17] This class of approximations introduces horizontal gradients of longitudinal (i.e., non-HP shear stress) components into the momentum balance equations. The main differences between the class members are the ways in which these stresses are approximated. Horizontal gradients of HP shear stresses are not included apart from one case where they are approximated, and the horizontal gradient of the vertical velocity is also neglected apart from one case. Thus in all but one member of this class the field equations are approximated by

$$\left.\begin{aligned} \partial_{\tilde{z}} \tilde{\tau}_{xz}^{(\mathrm{L}\cdot)} + \partial_{\tilde{x}} \tilde{\tau}_{xx}^{(\mathrm{L}\cdot)} + \partial_{\tilde{y}} \tilde{\tau}_{xy}^{(\mathrm{L}\cdot)} &= \partial_{\tilde{x}} \tilde{p}^{(\mathrm{L}\cdot)} - \tilde{\rho}\tilde{g}\varepsilon, \\ \partial_{\tilde{z}} \tilde{\tau}_{yz}^{(\mathrm{L}\cdot)} + \partial_{\tilde{y}} \tilde{\tau}_{yy}^{(\mathrm{L}\cdot)} + \partial_{\tilde{x}} \tilde{\tau}_{xy}^{(\mathrm{L}\cdot)} &= \partial_{\tilde{y}} \tilde{p}^{(\mathrm{L}\cdot)}, \\ \partial_{\tilde{z}} \tilde{\tau}_{zz}^{(\mathrm{L}\cdot)} &= \partial_{\tilde{z}} \tilde{p}^{(\mathrm{L}\cdot)} + \tilde{\rho}\tilde{g}, \end{aligned}\right\} \tag{14}$$

with boundary tractions given by

$$\left.\begin{aligned} \tilde{\tau}_{xz(s)}^{(\mathrm{L}\cdot)} + 2\partial_x \tilde{s}\tilde{\tau}_{xx(s)}^{(\mathrm{L}\cdot)} + \partial_y \tilde{s}\tilde{\tau}_{xy(s)}^{(\mathrm{L}\cdot)} &= 0, \\ \tilde{\tau}_{yz(s)}^{(\mathrm{L}\cdot)} + \partial_x \tilde{s}\tilde{\tau}_{xy(s)}^{(\mathrm{L}\cdot)} + 2\partial_y \tilde{s}\tilde{\tau}_{yy(s)}^{(\mathrm{L}\cdot)} &= 0, \\ \tilde{\sigma}_{zz(s)}^{(\mathrm{L}\cdot)} &= 0, \\ \tilde{\tau}_{xz(b)}^{(\mathrm{L}\cdot)} + 2\partial_x \tilde{b}\tilde{\tau}_{xx(b)}^{(\mathrm{L}\cdot)} + \partial_y \tilde{b}\tilde{\tau}_{xy(b)}^{(\mathrm{L}\cdot)} &= \tilde{T}_{tx(b)}^{(\mathrm{L}\cdot)}, \\ \tilde{\tau}_{yz(b)}^{(\mathrm{L}\cdot)} + \partial_x \tilde{b}\tilde{\tau}_{xy(b)}^{(\mathrm{L}\cdot)} + 2\partial_y \tilde{b}\tilde{\tau}_{yy(b)}^{(\mathrm{L}\cdot)} &= \tilde{T}_{ty(b)}^{(\mathrm{L}\cdot)}, \\ \tilde{\sigma}_{zz(b)}^{(\mathrm{L}\cdot)} &= \tilde{\tau}_{zz(b)}^{(\mathrm{L}\cdot)} - \tilde{p}^{(\mathrm{L}\cdot)}. \end{aligned}\right\} \tag{15}$$

3.2.1. (L1S1): One-Layer Longitudinal Stresses Using τ_{xx} at Surface Computed According to Shallow Ice Approximation

[18] In this approximation, longitudinal stresses are approximated by their values at the surface using a surface velocity field computed according the shallow approximation. Thus the momentum balance equations are approximated by equations (14) and (15), and the strain definitions and constitutive relationships are

$$\left.\begin{aligned} \tilde{e}_{jk(s)}^{(\mathrm{S})} &= \tilde{A}_c \tilde{\tau}_\ell^{(\mathrm{L1S1})n-1} \tilde{\tau}_{jk}^{(\mathrm{L1S1})}, \\ \tilde{e}_{jz}^{(\mathrm{L1S1})} &= \tfrac{1}{2}\partial_{\tilde{z}} \tilde{u}_j^{(\mathrm{L1S1})}, \\ \tilde{e}_{jz}^{(\mathrm{L1S1})} &= \tilde{A}_c \tilde{\tau}_s^{(\mathrm{L1S1})n-1} \tilde{\tau}_{jz}^{(\mathrm{L1S1})}. \end{aligned}\right\} \tag{16}$$

3.2.2. (L1S2): One-Layer Longitudinal Stresses Using e_{xx} at Surface Computed According to Shallow Ice Approximation, Vertical Correction of τ_{xx}

[19] In this approximation, non-HP strain rates are approximated by their values at the surface using a surface velocity field computed according the shallow approximation. Non-HP stresses are given by inserting the surface strain rate into the constitutive relationship, using the SIA horizontal plane shear stresses in the invariant and using the resulting nonlinear equation to solve for the longitudinal stress. This means that the momentum balance equations are approximated by equations (14) and (15), but the stretching relationships of equation (16) are replaced by

$$\left.\begin{aligned}
\tilde{\tau}^{(\mathrm{L1S2a})2} &= \tilde{\tau}_s^{(\mathrm{S})2} + \tilde{\tau}_\ell^{(\mathrm{L1S2})2},\\
\upsilon(\zeta)\tilde{e}_{jk(s)}^{(\mathrm{S})} &= \tilde{A}_c\tilde{\tau}^{(\mathrm{L1S2a})n-1}\tilde{\tau}_{jk}^{(\mathrm{L1S2})},\\
\tilde{\tau}^{(\mathrm{L1S2b})2} &= \tilde{\tau}_s^{(\mathrm{L1S2})2} + \tilde{\tau}_\ell^{(\mathrm{L1S2})2},\\
\tilde{e}_{jz}^{(\mathrm{L1S2})} &= \tfrac{1}{2}\partial_{\tilde{z}}\tilde{u}_j^{(\mathrm{L1S2})},\\
\tilde{e}_{jz}^{(\mathrm{L1S2})} &= \tilde{A}_c\tilde{\tau}^{(\mathrm{L1S2b})n-1}\tilde{\tau}_{jz}^{(\mathrm{L1S2})}.
\end{aligned}\right\} \tag{17}$$

Here, υ is a shape factor describing how the velocity might vary with depth. It is set to unity in the numerical computations for L1S2 in this paper.

3.2.3. (L1L1): One-Layer Longitudinal Stresses Using τ_{xx} at Surface Computed by Solving Elliptic Equations

[20] Here, the surface velocities used in computing the non-HP stresses are computed using the shear stresses $\tilde{\tau}_{jz}^{(\mathrm{L1L1})}$ in the shear strain relationship and in the sliding relationship, but otherwise, the algorithm is the same as for L1S1. If one excludes the within-ice deformational component of velocity, L1L1 is identical to the approximation used by *MacAyeal* [1989]. The momentum balance equations are thus approximated by equations (14) and (15), but the stretching relationships of equation (16) are replaced by

$$\left.\begin{aligned}
\tilde{e}_{jk(s)}^{(\mathrm{L1L1})} &= \tilde{A}_c\tilde{\tau}_\ell^{(\mathrm{L1L1})n-1}\tilde{\tau}_{jk}^{(\mathrm{L1L1})},\\
\tilde{e}_{jz}^{(\mathrm{L1L1})} &= \tfrac{1}{2}\partial_{\tilde{z}}\tilde{u}_j^{(\mathrm{L1L1})},\\
\tilde{e}_{jz}^{(\mathrm{L1L1})} &= \tilde{A}_c\tilde{\tau}_s^{(\mathrm{L1L1})n-1}\tilde{\tau}_{jz}^{(\mathrm{L1L1})}.
\end{aligned}\right\} \tag{18}$$

3.2.4. (L1L2): One-Layer Longitudinal Stresses Using ε_{xx} at Surface Computed by Solving Elliptic Equations, Vertical Correction of τ_{xx}

[21] Here, the surface velocities used in computing the non-HP stresses are computed using the shear stresses $\tilde{\tau}_{jz}^{(\mathrm{S})}$ in the shear strain relationship and in the sliding relationship, but otherwise, the algorithm is the same as for L1S2. The momentum balance equations are thus approximated by equations (14) and (15), but the stretching relationships of equation (16) are replaced by

$$\left.\begin{aligned}
\tilde{\tau}^{(\mathrm{L1L2a})2} &= \tilde{\tau}_s^{(\mathrm{S})2} + \tilde{\tau}_\ell^{(\mathrm{L1L2})2},\\
\upsilon(\zeta)\tilde{e}_{jk(s)}^{(\mathrm{L1L2})} &= \tilde{A}_c\tilde{\tau}^{(\mathrm{L1L2a})n-1}\tilde{\tau}_{jk}^{(\mathrm{L1L2})},\\
\tilde{\tau}^{(\mathrm{L1L2b})2} &= \tilde{\tau}_s^{(\mathrm{L1L2})2} + \tilde{\tau}_\ell^{(\mathrm{L1L2})2},\\
\tilde{e}_{jz}^{(\mathrm{L1L2})} &= \tfrac{1}{2}\partial_{\tilde{z}}\tilde{u}_j^{(\mathrm{L1L2})},\\
\tilde{e}_{jz}^{(\mathrm{L1L2})} &= \tilde{A}_c\tilde{\tau}^{(\mathrm{L1L2b})n-1}\tilde{\tau}_{jz}^{(\mathrm{L1L2})}.
\end{aligned}\right\} \tag{19}$$

Hindmarsh (submitted manuscript, 2004) shows that $\upsilon = 1$ is sufficient to produce a scheme with $O(\delta^2)$ accuracy. This value is used in the paper. A very slightly more accurate choice is $\upsilon = u_x^{(\mathrm{SIA})}/u_{x(s)}^{(\mathrm{SIA})}$, but the gain in accuracy is small compared with the other errors.

3.2.5. (LMLa): Multilayer Longitudinal Stresses

[22] This is the classic longitudinal stress scheme as used by *Blatter* [1995] and by *Pattyn* [2003]. The momentum balance equations are thus approximated by equations (14) and (15), but the stretching relationships of equation (16) are replaced by

$$\left.\begin{aligned}
\tilde{\tau}^{(\mathrm{LML}\cdot)2} &= \tilde{\tau}_s^{(\mathrm{LML}\cdot)2} + \tilde{\tau}_\ell^{(\mathrm{LML}\cdot)2},\\
\tilde{e}_{jk}^{(\mathrm{LML}\cdot)} &= \tilde{A}_c\tilde{\tau}^{(\mathrm{LML}\cdot)n-1}\tilde{\tau}_{jk}^{(\mathrm{LML}\cdot)},\\
\tilde{e}_{jz}^{(\mathrm{LMLa})} &= \tfrac{1}{2}\partial_{\tilde{z}}\tilde{u}_j^{(\mathrm{LMLa})},\\
\tilde{e}_{jz}^{(\mathrm{LML}\cdot)} &= \tilde{A}_c\tilde{\tau}^{(\mathrm{LML}\cdot)n-1}\tilde{\tau}_{jz}^{(\mathrm{LML}\cdot)}.
\end{aligned}\right\} \tag{20}$$

[23] Compared with L1L2, the longitudinal stresses use the velocity at the corresponding elevations rather than at the surface, and the stress-invariant calculations are self-consistent rather than using the SIA stress.

3.2.6. (LMLb): Multilayer Longitudinal Stresses With Full Shear Strain Relationship

[24] This is the same as LMLa, but the stretching relationships of equation (16) now include the horizontal gradient of $\tilde{w}$, and thus the shear strain definition is replaced by

$$\tilde{e}_{jz}^{(\mathrm{LMLb})} = \frac{1}{2}\left(\partial_{\tilde{z}}\tilde{u}_j^{(\mathrm{LMLb})} + \partial_{\tilde{j}}\tilde{w}^{(\mathrm{LMLb})}\right). \tag{21}$$

3.2.7. (LTSML): Multilayer Longitudinal Stresses With Horizontal Shear Stress Gradient Approximated by SIA

[25] Horizontal gradients of vertical velocity are neglected, so the shear relations are as equation (20). HP shear stresses, when needed to compute the horizontal gradient of such shear stresses, are approximated by SIA values. In consequence, the vertical momentum balance equation in the set of equation (14) is replaced by

$$\partial_{\tilde{x}}\tilde{\tau}_{xz}^{(\mathrm{S})} + \partial_{\tilde{y}}\tilde{\tau}_{yz}^{(\mathrm{S})} + \partial_{\tilde{z}}\tilde{\tau}_{zz}^{(\mathrm{LTSML})} = \partial_{\tilde{z}}\tilde{p}^{(\mathrm{LTSML})} + \tilde{\rho}\tilde{g}, \tag{22}$$

while the boundary conditions remain equation (15).

4. Scaling, Mapping, and Linearizations

[26] This paper deals with many distinct but closely related quantities, and the notation follows a fairly strict system. As explained in section 3, superscripts give information about the approximant being used, and readers are reminded that a superscript in parentheses containing a member of the set $\mathcal{A}$ shows that the superscripted quantity has been computed according to the corresponding approximation scheme. A superscript with parentheses containing 0 or 1 refers to the perturbation order in the linearization parameter μ introduced below in equation (24). These superscripts may appear together, in separate parentheses. Superscripts without parentheses always occur at the rightmost end of the superscript chain and are exponents. Sub-

scripts without parentheses occur at the leftmost end of the subscript chain. These can refer to tensor or vector components or to other quantities, which will be clear from the context. Parenthetic subscripts are either (s) or (b) and refer to evaluation of the quantity at the surface and the base, respectively. For example, $\tau^{(\mathrm{S})(1)2}_{xz(b)}$ is the dimensionless first-order horizontal plane shear stress in the x direction, raised to the power 2 and computed according to approximation scheme S (actually the SIA), evaluated at the base.

[27] The variables are nondimensionalized as follows. Thicknesses H, elevations z, s, and b, and horizontal positions $\mathbf{r} = (x, y)$ are scaled by $\tilde{H}_*$ (asterisk subscripts imply a scale magnitude). Dimensionless field quantities within the ice are expressed in a normalized vertical coordinate ζ, defined by

$$0 \le \zeta = \tilde{H}^{-1}\left(\tilde{z} - \tilde{b}\right) = H^{-1}(z - b) \le 1. \tag{23}$$

Hindmarsh and Hutter [1988] and *Hindmarsh* [1999] write out the associated differential transforms. In physical units the operators $\boldsymbol{\nabla}_{\mathrm{H}}\cdot$ and $\boldsymbol{\nabla}_{\mathrm{H}}$ act in the $(\tilde{\mathbf{r}}, \tilde{z})$ coordinate system, while in the dimensionless system they act in the $(\mathbf{r}, \zeta)$ system. Pressure and stresses are scaled by $\varepsilon\tilde{\rho}\tilde{g}\tilde{H}_*$, where $\tilde{g} = |\tilde{\mathbf{g}}|$ is the acceleration due to gravity. In dimensionless form the gravity vector $\mathbf{g}$ has components $(\varepsilon, 0, -1)$, where $\varepsilon^2 \ll 1$. The velocity scale $\tilde{v}_*$ is chosen so as to set $u^{(\mathrm{S})(0)}_{x(s)} = 1$. The accumulation rate a and the velocity $\mathbf{v}$ are scaled by $\tilde{v}_*$, the flux has scale given by $\tilde{q}_* = \tilde{v}_*\tilde{H}_*$, and time is scaled by $\tilde{t}_* = \tilde{H}_*/\tilde{v}_*$. These scalings imply $\tilde{A}^*_c = \tilde{v}_*/(\tilde{H}_*\tilde{\tau}^{*n})$ and $\tilde{A}^*_s = \tilde{v}_*/\tilde{\tau}^{*(\ell-\nu)}$.

[28] The relevant field variables are subsequently linearized with a small parameter μ about a base case solution (steady uniform flow down the infinite plane), for example,

$$H = H^{(0)} + \mu H^{(1)}(\mathbf{r}, t), \mathbf{v} = \mathbf{v}^{(0)} + \mu\mathbf{v}^{(1)}(\mathbf{r}, \zeta, t), \tag{24}$$

etc. These are used to derive a set of zeroth-order and first-order equations expressing conservation of mass and momentum. A Fourier transform in the horizontal plane is then applied to the first-order equations, and the first-order fields can be expressed as plane waves:

$$\left.\begin{aligned} H^{(1)} &= \Re\left\{\hat{H}^{(1)}\exp(\lambda t - \mathrm{i}\mathbf{k}\cdot\mathbf{r})\right\},\\ \mathbf{v}^{(1)} &= \Re\left\{\hat{\mathbf{v}}^{(1)}(\zeta)\exp(\lambda t - \mathrm{i}\mathbf{k}\cdot\mathbf{r})\right\},\end{aligned}\right\} \tag{25}$$

etc. In particular, $\hat{H}^{(1)} = \hat{s}^{(1)} - \hat{b}^{(1)}$. In equation (25), λ is the eigenvalue, the wave numbers are given by $\mathbf{k} = (k_x, k_y)$, and the caret indicates the Fourier coefficient of the transform over the $\mathbf{r}$-plane only. The scaling is constructed to ensure that H_0 and as many as is possible of the other zeroth-order quantities are unity. The eigenvalue λ is, in general, a complex number. The real part gives the growth rate, with negative values indicating decay. The imaginary part, when divided by the wave number, gives the wave speed.

[29] After applying the linearization of equation (24), with the assumption of quasi-uniform base flow, one finds that

$$\boldsymbol{\tau}^{(0)} = \begin{bmatrix} \tau^{(0)}_{xx} & 0 & \tau^{(0)}_{xz}\\ 0 & 0 & 0\\ \tau^{(0)}_{xz} & 0 & \tau^{(0)}_{zz}\end{bmatrix}. \tag{26}$$

The zeroth-order momentum balance equations are

$$\partial_\zeta\tau^{(0)}_{xz} = -1, \qquad \partial_\zeta p^{(0)} = -1/\varepsilon, \tag{27}$$

and the linearized zeroth-order strain-rates are

$$\mathbf{e}^{(0)} = \begin{bmatrix} \alpha u^{(0)}_x & 0 & \frac{1}{2}\partial_\zeta u^{(0)}_x\\ 0 & 0 & 0\\ \frac{1}{2}\partial_\zeta u^{(0)}_x & 0 & -\alpha u^{(0)}_x\end{bmatrix}. \tag{28}$$

The strain rates e_{xx} and e_{zz} are therefore directly proportional to the horizontal velocity. The quantity α is chosen to ensure that $w^{(0)}_s + a = 0$. The strain rate invariants e and $e^{(0)}$ are given by

$$\left.\begin{aligned} 2e^2 &= 2e^2_{xz} + 2e^2_{yz} + 2e^2_{xy} + e^2_{xx} + e^2_{yy} + e^2_{zz},\\ e^{(0)2} &= e^{(0)2}_{xz} + e^{(0)2}_{xx},\end{aligned}\right\} \tag{29}$$

and constitutive relationships are conveniently written in terms of a viscosity

$$\left.\begin{aligned} \boldsymbol{\tau} &= 2\eta\mathbf{e}, \qquad \eta = Be^{\frac{1}{n}-1},\\ \boldsymbol{\tau}^{(0)} &= 2\eta^{(0)}\mathbf{e}^{(0)}, \quad \eta^{(0)} = Be^{(0)\frac{1}{n}-1},\\ B &= A_c^{-\frac{1}{n}}/2.\end{aligned}\right\} \tag{30}$$

At the surface the zeroth-order boundary conditions are

$$\tau^{(0)}_{xz(s)} = 0, \qquad \tau^{(0)}_{yz(s)} = 0, \qquad \sigma^{(0)}_{zz(s)} = 0, \tag{31}$$

while at the base they are

$$\left.\begin{aligned} \tau^{(0)}_{jz(b)} &= T^{(0)}_{tj(b)},\\ \sigma^{(0)}_{zz(b)} &= T^{(0)}_{n(b)}, \qquad w^{(0)}_{(b)} = 0,\\ \mathbf{u}^{(0)}_{(b)} &= A_c\left|\mathbf{T}^{(0)}_{t(b)}\right|^{\ell-1}\mathbf{T}^{(0)}_{t(b)}/p^{(0)\lambda}_e.\end{aligned}\right\} \tag{32}$$

The zeroth-order solution is similar to the shallow ice approximation, but the assumption of quasi-uniform flow creates some differences as the tensor components $\tau^{(0)}_{xx}$, $\tau^{(0)}_{zz}$, $e^{(0)}_{xx}$, and $e^{(0)}_{zz}$ contribute to the respective invariants and hence to the viscosity. The nonlinear equation set

$$\left.\begin{aligned} \tau^{(0)}_{xz} &= 1 - \zeta, \qquad \eta^{(0)} = Be^{(0)\frac{1}{n}-1},\\ e^{(0)2} &= e^{(0)2}_{xz} + e^{(0)2}_{xx}, \qquad e^{(0)}_{xx} = \alpha u^{(0)}/u^{(0)}_{(s)},\\ u^{(0)} &= \int_0^\zeta \tfrac{\tau^{(0)}_{xz}}{\eta^{(0)}}\mathrm{d}\zeta + u^{(0)}_{(b)},\\ w^{(0)} &= \int_0^\zeta e^{(0)}_{xx}\mathrm{d}\zeta, \qquad w^{(0)}_{(s)} = -a^{(0)},\end{aligned}\right\} \tag{33}$$

with boundary conditions equations (31) and (32) is solved by a direct iteration starting from the shallow ice approximation. The computation of α forms part of the

iteration, ensuring that the vertical velocity balances the accumulation rate at the upper surface. This procedure also incorporates longitudinal stretching into the viscosity calculation. The assumption of quasi-uniform flow means that we treat $u_x^{(0)}$ as being independent of x, even though it is not; $\partial_x u_x^{(0)}$ is actually nonzero, but the product of $\partial_x u_x^{(0)}$ and the wavelength of interest is small. This construction avoids the difficulties of having a singular $\eta^{(0)}$ at the upper surface.

[30] The first-order equations are given in Appendix A. The combination of equations (30), (A1), (A3), (A8), and (A9) leads to a linear eigenvalue problem, which is solved using pseudo-spectral methods [*Fornberg*, 1996]. Details of the implementation follow examples given by *Trefethen* [2000]. The solution gives the eigenvalue λ as a function of k_x, k_y. Twenty-one Chebyshev points were used in the discretization, which gives very high accuracy in the numerical solution. The parameters of the problem are the downstream body-force component ε, the rheological indices n, ℓ, and ν, the slip ratio (the ratio of the sliding velocity to the difference between surface and basal velocity) specified by varying A_c, and the accumulation rate (which affects the parameter α).

[31] To compute the eigenvalue, one also needs the flux

$$\hat{\mathbf{Q}}^{(1)} = \frac{\hat{H}^{(1)}}{H^{(0)}}\mathbf{Q}^{(0)} + H^{(0)}\int_0^1 \hat{\mathbf{u}}^{(1)}\mathrm{d}\zeta, \tag{34}$$

which depends linearly upon $\hat{H}^{(1)}$. The first-order continuity equation in Fourier space is

$$\lambda\hat{H}^{(1)} - i\mathbf{k}\cdot\hat{\mathbf{Q}}^{(1)} = \hat{a}^{(1)}. \tag{35}$$

[32] Cases LMLa, LMLb, and LTSML can be represented in the numerical eigenvalue solver by minor code adjustments. Cases S, L1S1, L1S2, L1L1, and L1L2 are more conveniently performed semianalytically using quadratures. Case S has analytical solutions discussed by, e.g., *Gudmundsson* [2003]. The horizontal velocities, which can be substituted into equation (34), are given by equations (B5), (B18), (B4), and (B17), respectively.

5. Comparisons

5.1. Comparison With Analytical Solution for Newtonian Rheology

[33] *Gudmundsson* [2003] gives a solution for the linearized free-surface flow of a Newtonian fluid down the infinite plane. Analytical spectra (i.e., the dependence of $\Re(\lambda)$ on the wavelength vector $\mathbf{L} = (L_x, L_y)$) computed using this solution can be compared with those computed using the numerical eigensolver described in section 4. Results of the comparison are shown in Figure 2. In this case and in all cases reported here the bed is assumed to be undeforming ($\partial_t b^{(1)}(\mathbf{r}, t) = 0$) and the first-order accumulation rate $\hat{a}^{(1)} = 0$.

[34] As usually happens with free-surface flows, the slope of the spectrum $\partial\Re(\lambda)/\partial L_x$ or $\partial\Re(\lambda)/\partial L_y$ depends upon the wavelength, with the fastest decay (most negative value of $\Re(\lambda)$) occurring at wavelengths comparable with the thickness of the fluid. For smaller wavelengths the slope is negative, while for larger wavelengths the slope is positive. This is shown in Figure 2a. An excellent fit between analytical and numerical solutions is found, on account of the very high accuracy spectral method being used. *Gudmundsson* [2003] showed that for high slip ratio, the maximum decay rate occurs for an extended band of wavelengths, starting at a wavelength around the ice sheet thickness (Figure 2c). The eigensolver is equally accurate under these conditions.

[35] For plane flow the kinematic wave speed is given by $\Im(\lambda)/k_x$. At long wavelengths the kinematic wave speed is $n + 1$ or $\nu + 1$ times the surface velocity (unity in the present scaling) for the extremes of zero slip and perfect slip, while at short wavelength, waves are passively advected, with wave speed unity in this scaling. Figures 2b and 2d demonstrate excellent fits between the numerical Stokes solver and the analytical solution for the imaginary component of the eigenvalue.

[36] Figure 2 also shows a comparison between the numerical solution of model LMLa and an analytical solution for this model when the rheology is linear. The derivation is outlined in Appendix C. For the real part of the eigenvalue (Figures 2a and 2c) the fit is excellent. When one considers the wave velocity (Figures 2b and 2d) for flow with no slip, the analytical solution for LMLa and the numerical solution show some divergence at shorter (less than unity) wavelengths, although this is not apparent for flow with sliding. The high-accuracy spectral scheme being used suggests that this divergence is not due to numerical truncation error, and it should be taken as a caution that the computation of wave motion and phasing may be more sensitive to errors at shorter wavelengths. This will be seen to be a general pattern.

[37] Both analytical solutions have been obtained by applying the boundary conditions at the perturbed position of the surfaces and do not have any coordinate stretching terms. The closeness of fit strongly suggests that having a perturbed coordinate system does not affect the accuracy of the solution for the real part of the solution, although this may not be the case for the imaginary part. From a dynamical aspect the rapid decay of perturbations means that kinematic waves move very short distances before disappearing [*Gudmundsson*, 2003], so the relative inaccuracy involved in the computation of the imaginary component is probably not important in the dynamic response. However, the amplitude and phasing of steady surface profiles with respect to basal profiles are, in principle, affected by both components and will be considered more closely in the comparisons for a nonlinear rheology that follow (section 5.2).

5.2. Comparisons for Glen Rheologies, Varying Slip Ratios

[38] The main purpose of this paper is now reached, where spectra and other response descriptors from Stokes equations approximants are compared with those for the full Stokes equations. In all the many cases investigated (most not reported here in detail), there is no indication of any instability (a positive eigenvalue). Results are shown in Figures 3 (no slip), 4 (moderate slip), and 5 (very high slip). These cases are for a Glen rheology, with the Stokes equations spectra obtained numerically. The results are quoted in dimensionless units but roughly correspond to a glacier with $\tilde{A}_c = 5 \times 10^{-24}$ Pa^{-3} s, $\tilde{a} = 0.1$ m yr^{-1}, $\tilde{\rho} = 917$ kg m^{-3}, $\tilde{g} =$

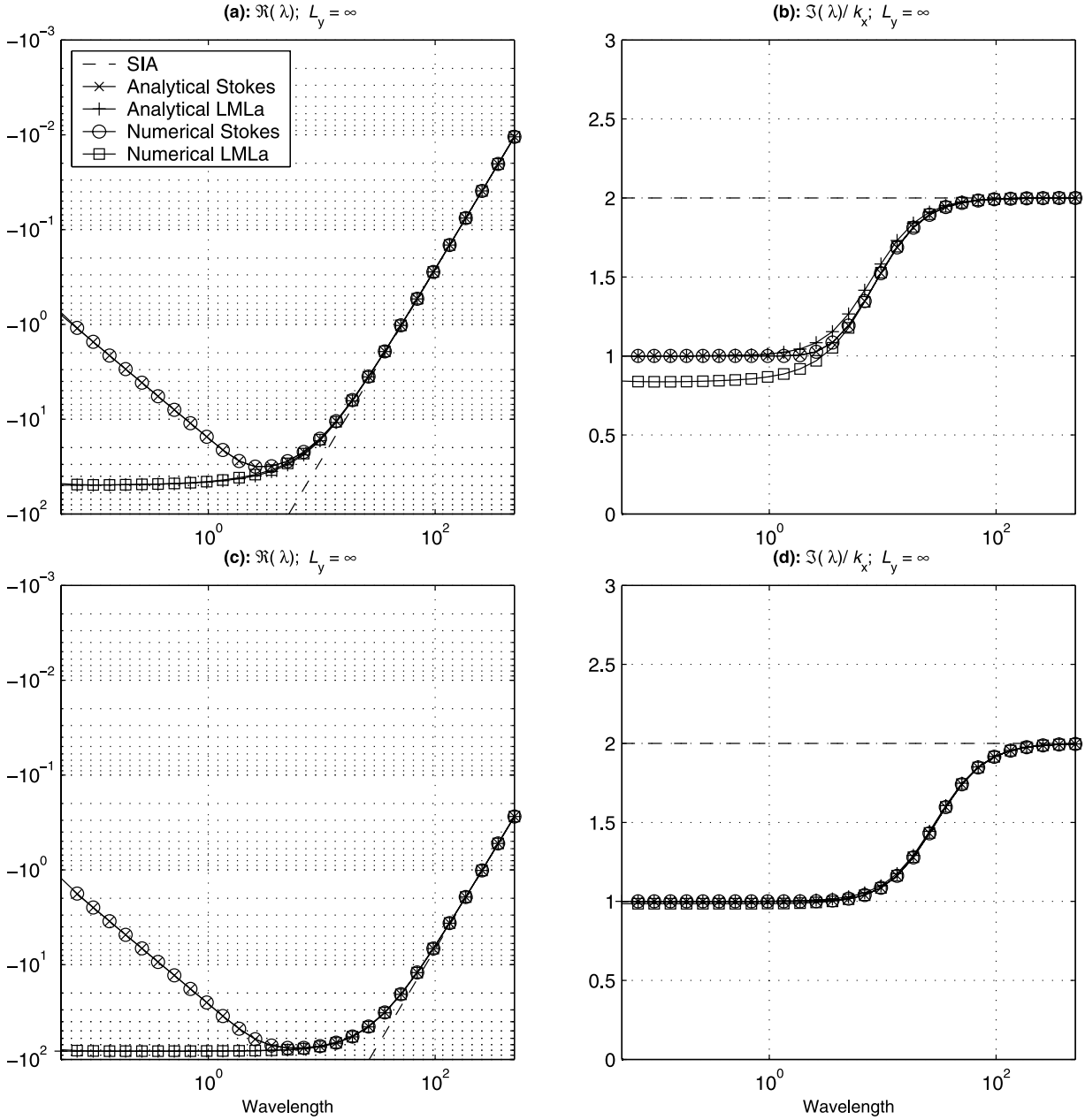

Figure 2. Comparison of numerical solutions with analytical solutions for a Newtonian rheology, for full Stokes systems [*Gudmundsson*, 2003], and for model LMLa (Appendix C). (a, c) Growth rate $\Re(\lambda)$. (b, d) Wave speed $\Im(\lambda)/|\mathbf{k}|$ plotted as a function of the wavelength $L_x = 2\pi/k$. The transverse wavelength $L_y = \infty$. Parameters $n = 1$, $a = 0$, $\ell = 1$, and $\nu = 0$. Figures 2a and 2b are for no slip, $\epsilon = 0.01$; Figures 2c and 2d are for slip ratio 10, $\epsilon = 0.00056$. Note that analytical and numerical solutions are virtually coincident for the full Stokes system and the approximant LMLa. Also note that analytical and numerical solutions are superimposed in all panels except Figure 2b.

9.81 m s^{-2}, and $\tilde{H} = 2000$ m. The parameters as specified create an upper surface velocity of roughly 5×10^2 m yr^{-1}.

[39] Four response descriptors are analyzed; the growth rate $\Re(\lambda)$, the wave speed $\Im(\lambda)/|\mathbf{k}|$, the steady state surface response $|s^{(1)}(t \to \infty)/b^{(1)}|$, and the steady state surface phasing arg $(s^{(1)}\ (t \to \infty)/b^{(1)})$. Figures 3 and 5 show these quantities plotted as a function of $L_x = 2\pi/k_x$. Figure 4 shows four spectra, two as a function of the x wavelength, the other two as a function of the y wavelength. The orthogonal wavelength is kept constant either at infinity or at ten ice thicknesses. These quantities are all plotted as for $L_x \geq 1$.

[40] In all cases shown, the general pattern of the Stokes equation spectrum (i.e., $\Re(\lambda)$ plotted as a function of L_j) is the same as for the linear rheology. For smaller wavelengths the slope is negative, while for larger wavelengths the slope is positive. For the Newtonian case the curvature (in log-log space) is always positive, but for the Glen rheology, there are points of inflexion on the ascending branch, at intermediate wavelengths. In this case the SIA is a substantially

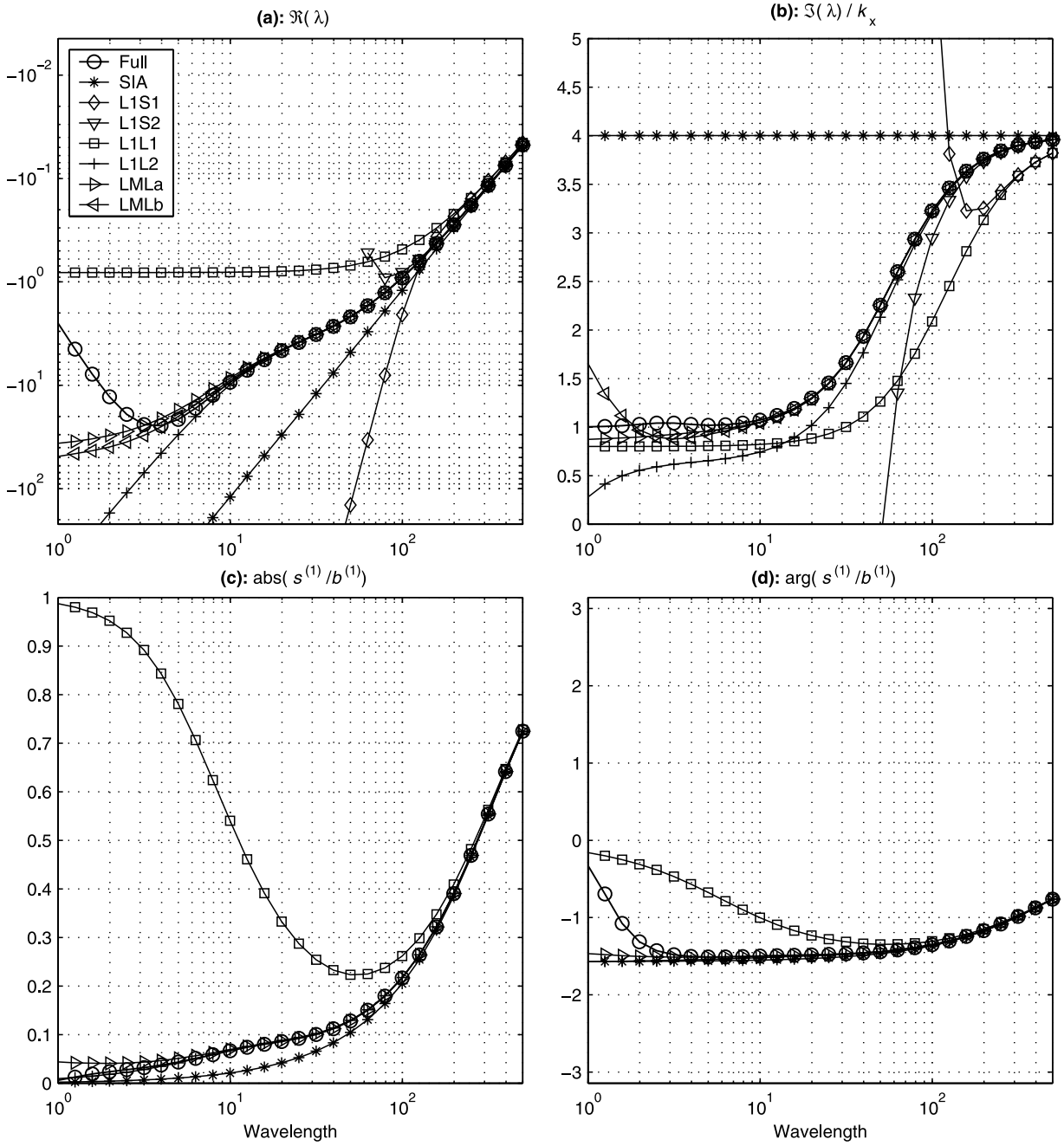

Figure 3. Response of the different indicated parameters for different approximants (see section 3 for definitions) plotted as a function of wavelength L_x. (a) Growth rate. (b) Kinematic wave velocity. (c) Transfer amplitude for steady flow. (d) Transfer phasing for steady flow. Flow occurs without slip and with internal deformation according to a Glen rheology. Case L1L2 is not plotted in certain regions because of instability (positive eigenvalue); cases L1S1, L1S2, and LMLb are not plotted in Figures 3c and 3d. Parameters are $n = 3$, $a = 2 \times 10^{-4}$, $\varepsilon = 0.0079$, $\ell = 3$, and $\nu = 0$. Note the extensive superimposing of different lines for wavelengths ≥ 5.

worse approximation than the Newtonian case, departing from the Stokes spectrum at wavelengths of around 10^2 ice sheet thicknesses, as compared with 10^1 for the Newtonian case. This effect is even more severe for high slip ratios. *Johannesson* [1992] noticed and commented on the deleterious effects of nonlinear rheologies on the SIA.

[41] As expected, accuracy of the L approximants compared with the full Stokes equations is poor for $L_x < 1$. However, apart from two cases mentioned below, where the approximants produce spurious instabilities, for wavelengths less than unity the decay rate is quicker for the approximants than for the full system, a feature exhibited in Figure 2. This is a desirable feature as it means that noise will decay more quickly than signal.

[42] The approximants L1S1 and L1S2 are not good. While L1S1 is better than the SIA over a certain band of

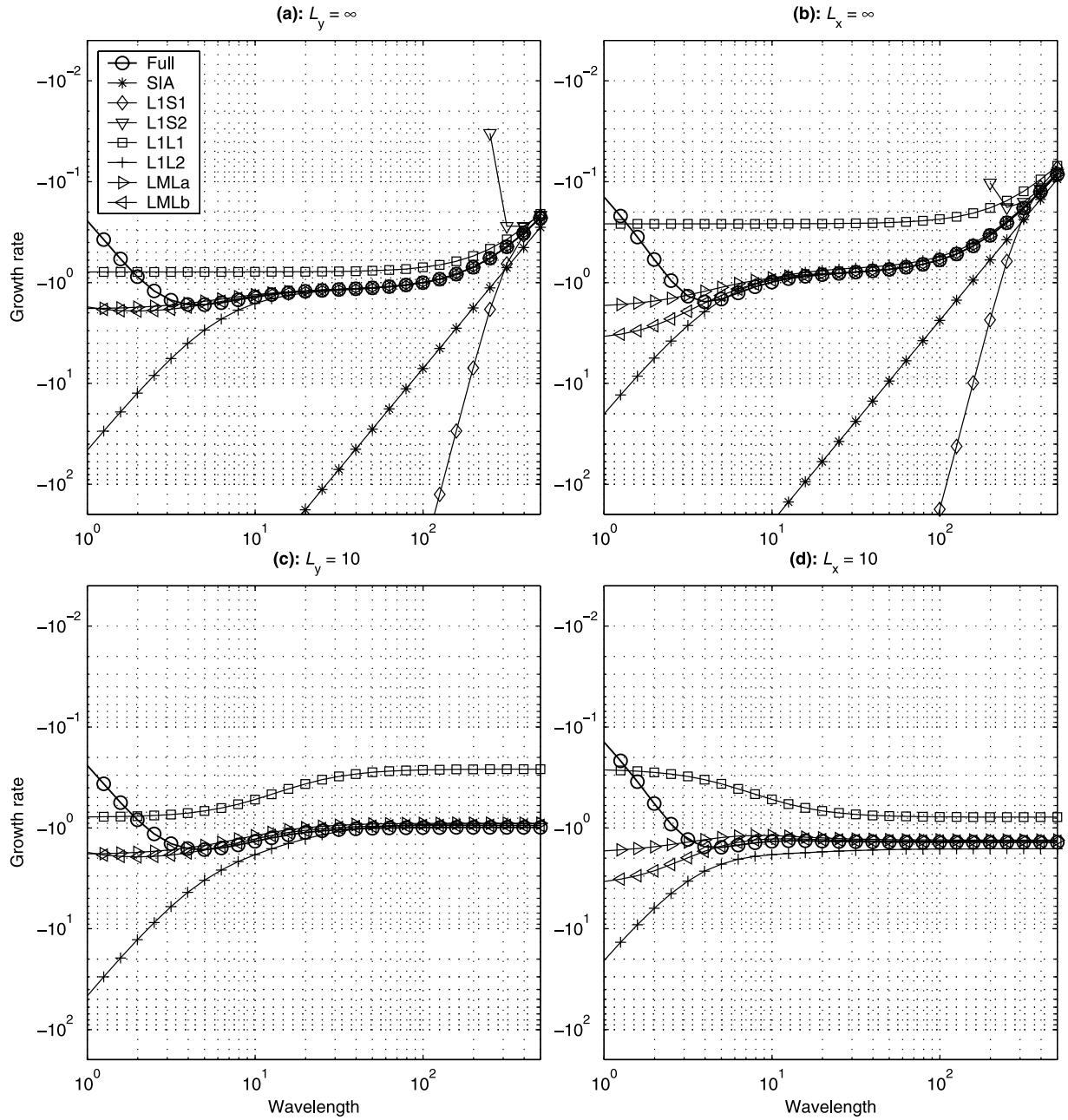

Figure 4. Growth rate $\Re(\lambda)$ for different approximants as a function of one of the wavelength components (L_x, L_y) for sliding with moderate slip ratio = 1.17×10^2. Constant wavelengths and directions are indicated in the titles: abscissae for (a and c) the x wavelength and for (b and d) the y wavelength. Parameters are $n = 3$, $a = 2 \times 10^{-4}$, $\varepsilon = 0.0017$, $\ell = 3$, and $\nu = 0$. Note the extensive superimposing of different lines for wavelengths ≥ 5.

wavelengths, at shorter wavelengths it becomes very much more inaccurate. L1S2 is dangerous, becoming unstable at quite long wavelengths (positive values not shown on the log-log plot).

[43] The single-layer approximant L1L1 is stable but generally not very accurate except at very high slip ratio. Since this is the mechanical model used in the shelf approximation, this is not unexpected. The approximation generally underestimates the rate of decay, which means that errors will persist. A closer investigation suggests that the problem lies in the use of the surface viscosity, which can be far too high.

[44] The multilayer approximant LMLb is generally very good, but can become unstable at wavelengths less than the ice thickness (not shown) and for this reason should be avoided. Of course, one would not be using this approximant to model short wavelength features, but this instability might be expected to wreak havoc in numerical schemes. Not shown in the graph is the approximant LTSML. This is also unstable at wavelengths less than the ice thickness and should also be avoided.

[45] This leaves the single-layer approximant L1L2 and the multilayer approximant LMLa. They represent the

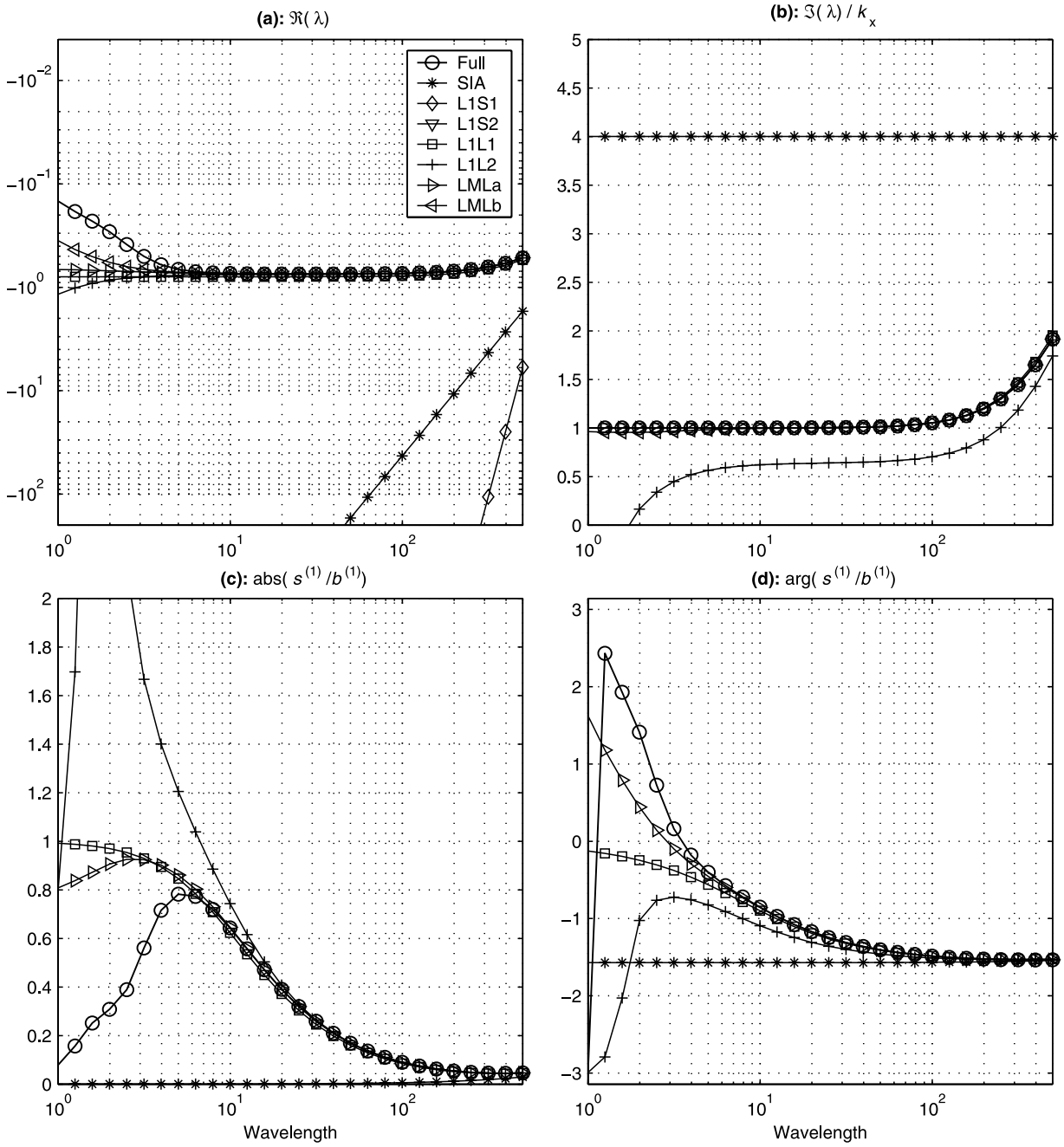

Figure 5. Response parameters ((a) growth rate, (b) kinematic wave velocity, (c) transfer amplitude for steady flow, and (d) transfer phasing for steady flow) for different approximants plotted as a function of wavelength L_x for sliding with very high slip ratio 6.19×10^3. Parameters are $n = 3$, $a = 2 \times 10^{-4}$, $\varepsilon = 0.00028$, $\ell = 3$, and $\nu = 0$. Other details are as for Figure 3. Note the extensive superimposing of different lines for wavelengths ≥ 5.

wavelength dependence of the spectrum very well to quite near the point of maximum decay rate. Both fail to capture the descending branch at short (subice thickness) wavelengths, as expected. The multilayer scheme is generally more accurate at shorter wavelengths but not overwhelmingly so. Both methods are reasonably accurate down to about five ice sheet thicknesses.

[46] At high slip ratios the extended band of maximum decay rate is found for nonlinear rheologies. The conclusions reached above about the relative merits of the different approximation schemes hold for the high-slip case as well.

[47] Turning now to the other response descriptors $\Im(\lambda)/|\mathbf{k}|$, $|s^{(1)}(t \to \infty)/b^{(1)}|$, and arg $(s^{(1)}\ (t \to \infty)/b^{(1)})$, shown in Figures 3 and 5, one sees that only approximants LMLa and LMLb perform consistently well for these descriptors. L1L1 is rather inaccurate at low slip ratios, while L1L2 is not of high accuracy at very high slip ratios. This occurs at short wavelengths, and even at high slip ratios, L1L2 looks useable down to about ten ice sheet thicknesses or possibly

better. In a practical implementation, L1L1 and L1L2 could be used in different zones depending on the slip ratio.

6. Discussion and Conclusions

[48] This paper contains an analysis, somewhat more comprehensive than previous studies, of how the inclusion of longitudinal stress effects improve the shallow ice approximation. In particular, it contains the first quantitative comparison of these approximants with each other and the full Stokes equations over the relevant wavelengths. This has been accomplished by the solution of a numerical eigenvalue problem. These solutions are sufficiently accurate to be certain that the differences in the results of the Stokes equations approximant are not contaminated with numerical truncation error. The numerical method has been compared with an analytical solution owing to *Gudmundsson* [2003], and the good agreement with spectra from the approximant L1L2, whose computation does not involve the solution of a numerical eigenvalue problem, is another source of confidence in the eigensolution.

[49] It is clear that inclusion of longitudinal stresses does force ice sheet dynamics to be closer to those associated with full solutions of the Stokes equations. As has been long believed, inclusion of longitudinal stresses increases accuracy at shorter wavelengths. Two schemes, a multilayer scheme and a single-layer scheme, are particularly good, with the single-layer scheme being nearly as good as the multilayer scheme. If this statement holds true for cases involving larger perturbations, this will permit considerable computational savings by reducing the dimensionality of the computational problem. In the examples shown in this paper, the use of longitudinal stress schemes increases accuracy at smaller wavelengths by a factor of around 20 compared with the SIA.

[50] Even though asymptotic analysis shows that the horizontal shear stress gradients are similarly ordered to longitudinal stress effects in sheet flow, computations show, in agreement with glaciological belief, that representing longitudinal stress terms alone improves the approximation considerably. Two longitudinal stress schemes, L1L2 and LMLa, are adequate approximations. LMLa is the computationally three-dimensional scheme used by, e.g., *Blatter* [1995] and *Pattyn* [2003]. It is slightly more accurate than L1L2, but L1L2 has the advantage that it is computationally two-dimensional as it is a vertically integrated model. More testing is needed to see whether the slightly lesser accuracy of L1L2 proves significantly deleterious in situations more general than small departures from uniformity. There is also a warning that some other plausible approximations introduce nonphysical instabilities and are potentially dangerous; approximation schemes should not be introduced without undergoing the testing described in this paper.

[51] The SIA can be used to model long-wavelength flows at low slip ratios. Once slip ratios become large, or wavelengths short, longitudinal stress approximations need to be included. This is known for the Newtonian rheology case from work by, e.g., *Gudmundsson* [2003], but guidance as to whether a particular case requires correction for longitudinal stress effects for a nonlinear case can be obtained by carrying out the analysis described in this paper. At wavelengths less than around five times the ice thickness, relaxation rates start to decrease as wavelength decreases; the maximum wavelength for this behavior is not strongly affected by the slip ratio. This behavior is represented by neither the SIA or with longitudinal stress schemes, and here, the full Stokes equations must be solved.

Appendix A: Linearized Stokes Equations

[52] The equations in this section may be derived from the governing equations by linearizing and performing a Fourier transform. The algebraic process is straightforward, and we simply quote the results. The first-order Fourier-transformed momentum balance equations are

$$\left.\begin{aligned} \partial_\zeta \hat{\tau}_{xz}^{(1)} - \mathrm{i}k_x \hat{\tau}_{xx}^{(1)} - \mathrm{i}k_y \hat{\tau}_{xy}^{(1)} + \mathrm{i}k_x \hat{p}^{(1)} \\ = -\mathrm{i}k_x \partial_\zeta p^{(0)} \hat{Z}^{(1)} + H^{(1)} \partial_\zeta \tau_{xz}^{(0)} + \mathrm{i}k_x \partial_\zeta \tau_{xx}^{(0)} \hat{Z}^{(1)}, \\ \partial_\zeta \hat{\tau}_{yz}^{(1)} - \mathrm{i}k_y \hat{\tau}_{yy}^{(1)} - \mathrm{i}k_x \hat{\tau}_{xy}^{(1)} + \mathrm{i}k_y \hat{p}^{(1)} \\ = -\mathrm{i}k_y \partial_\zeta p^{(0)} \hat{Z}^{(1)}, \\ \partial_\zeta \hat{\tau}_{zz}^{(1)} - \mathrm{i}k_x \hat{\tau}_{xz}^{(1)} - \mathrm{i}k_y \hat{\tau}_{yz}^{(1)} - \partial_\zeta \hat{p}^{(1)} \\ = -H^{(1)} \partial_\zeta p^{(0)} + \mathrm{i}k_x \partial_\zeta \tau_{xz}^{(0)} \hat{Z}^{(1)}, \end{aligned}\right\} \tag{A1}$$

where

$$\left.\begin{aligned} Z^{(1)} &= -\left(\zeta H^{(1)} + b^{(1)}\right), \\ \partial_x Z^{(1)} &= -\partial_x b^{(1)} - \zeta \partial_x H^{(1)}. \end{aligned}\right\} \tag{A2}$$

The first-order Fourier-transformed strain rates are

$$\left.\begin{aligned} \hat{e}_{xx}^{(1)} &= -\mathrm{i}k_x \left(\hat{u}^{(1)} + (1+\alpha)\hat{U}^{(1)}\right), \\ \hat{e}_{xy}^{(1)} &= -\tfrac{\mathrm{i}}{2}\left(k_x \hat{v}^{(1)} + k_y \left\{\hat{u}^{(1)} + \hat{U}^{(1)}\right\}\right), \\ \hat{e}_{xz}^{(1)} &= \tfrac{1}{2}\left(\partial_\zeta \hat{u}^{(1)} - \hat{U}^{*(1)} - \mathrm{i}k_x \left\{\hat{w}^{(1)} + \hat{W}^{(1)}\right\}\right), \\ \hat{e}_{yy}^{(1)} &= -\mathrm{i}k_y \hat{v}^{(1)}, \\ \hat{e}_{yz}^{(1)} &= \tfrac{1}{2}\left(\partial_\zeta \hat{v}^{(1)} - \mathrm{i}k_y \left\{\hat{w}^{(1)} + \hat{W}^{(1)}\right\}\right), \\ \hat{e}_{zz}^{(1)} &= \partial_\zeta \hat{w}^{(1)} - \hat{W}^{*(1)} + \mathrm{i}k_x \alpha \hat{U}^{(1)}, \end{aligned}\right\} \tag{A3}$$

where

$$\left.\begin{aligned} \hat{U}^{(1)} &= \partial_\zeta u^{(0)} \hat{Z}^{(1)}, \qquad \hat{W}^{(1)} = \partial_\zeta w^{(0)} \hat{Z}^{(1)}, \\ \hat{U}^{*(1)} &= \partial_\zeta u^{(0)} \hat{H}^{(1)}, \quad \hat{W}^{*(1)} = \partial_\zeta w^{(0)} \hat{H}^{(1)}. \end{aligned}\right\} \tag{A4}$$

At first order the strain rate invariant is

$$2e^{(0)}\hat{e}^{(1)} = 2e_{xz}^{(0)}\hat{e}_{xz}^{(1)} + e_{xx}^{(0)}\hat{e}_{xx}^{(1)} - e_{xx}^{(0)}\hat{e}_{zz}^{(1)}, \tag{A5}$$

and the first-order viscosity is given by

$$\hat{\eta}^{(1)} = \frac{1-n}{n}\frac{\eta^{(0)}}{e^{(0)2}}\left(e_{xz}^{(0)}\hat{e}_{xz}^{(1)} + \frac{1}{2}e_{xx}^{(0)}\left(\hat{e}_{xx}^{(1)} - \hat{e}_{zz}^{(1)}\right)\right). \tag{A6}$$

The first-order constitutive relationship is

$$\boldsymbol{\tau}^{(1)} = 2\eta^{(0)}\mathbf{e}^{(1)} + 2\eta^{(1)}\mathbf{e}^{(0)}. \tag{A7}$$

The first-order Fourier-transformed upper-surface boundary conditions are

$$\left.\begin{aligned} \hat{\tau}^{(1)}_{xz(s)} + 2\mathrm{i}k_x\hat{s}^{(1)}\tau^{(0)}_{xx(s)} &= 0,\\ \tau^{(1)}_{yz(s)} &= 0,\\ \hat{\sigma}^{(1)}_{zz(s)} + 2\mathrm{i}k_x\hat{s}^{(1)}\tau^{(0)}_{xz(s)} &= 0, \end{aligned}\right\} \tag{A8}$$

while the first-order Fourier-transformed basal boundary conditions are

$$\left.\begin{aligned} &\hat{T}^{(1)}_{tx(b)} = \hat{\tau}^{(1)}_{xz(b)} + 2\mathrm{i}k_x\hat{b}^{(1)}\tau^{(0)}_{xx(b)}, \quad \hat{T}^{(1)}_{ty(b)} = \tau^{(1)}_{yz(b)},\\ &\hat{T}^{(1)}_{n(b)} = \hat{\sigma}^{(1)}_{zz(b)} + 2\mathrm{i}k_x\hat{b}^{(1)}\tau^{(0)}_{xz(b)},\\ &\hat{\mathbf{u}}^{(1)}_{(b)} = \mathbf{R}_t\hat{\mathbf{T}}^{(1)}_{t(b)} + R_n\hat{T}^{(1)}_{n(b)}, \qquad \hat{w}^{(1)}_{(b)} = -\mathrm{i}\hat{b}^{(1)}\mathbf{u}^{(0)}_{(b)}\cdot\boldsymbol{k}, \end{aligned}\right\} \tag{A9}$$

where the quantities $\mathbf{R}_t = (R_{tx}, R_{ty})$, R_n are the linearized coefficients for the sliding law, as given by *Hindmarsh* [1998, equation (19)].

Appendix B: Spectra for Stokes Equations Approximants

[53] In this document, some single-layer longitudinal stress theories are subjected to a first-order perturbation. Where results are quoted explicitly as integrals, this indicates that they were evaluated numerically using spectral integration [*Trefethen*, 2000].

B1. LIL1, L1S1

[54] Linearizing and dropping the (L1L1) superscripts, the first-order equations momentum balance equations in Fourier space are

$$\left.\begin{aligned} \partial_\zeta\hat{\tau}^{(1)}_{xz} - 2\mathrm{i}k_x\hat{\tau}^{(1)}_{xx(s)} - \mathrm{i}k_y\hat{\tau}^{(1)}_{xy(s)} &=\\ -\mathrm{i}k_x\rho g\hat{s}^{(1)} + \hat{H}^{(1)}\partial_\zeta\tau^{(0)}_{xz},&\\ \partial_\zeta\hat{\tau}^{(1)}_{yz} - 2\mathrm{i}k_y\hat{\tau}^{(1)}_{yy(s)} - \mathrm{i}k_x\hat{\tau}^{(1)}_{xy(s)} &=\\ -\mathrm{i}k_y\rho g\hat{s}^{(1)},& \end{aligned}\right\} \tag{B1}$$

and the constitutive relationships are

$$\left.\begin{aligned} \hat{\tau}^{(1)}_{jk} &= \tfrac{1}{n}Be^{(0)m}_{xx(s)}\hat{e}^{(1)}_{jk(s)},\\ \partial_\zeta\hat{u}^{(1)}_x &= 2nA\tau^{(0)n-1}_{xz}\hat{\tau}^{(1)}_{xz} + \hat{H}^{(1)}\partial_\zeta u^{(0)}_x,\\ \partial_\zeta\hat{u}^{(1)}_y &= 2A\tau^{(0)n-1}_{xz}\hat{\tau}^{(1)}_{yz},\\ m &= \tfrac{1}{n} - 1. \end{aligned}\right\} \tag{B2}$$

Letting

$$\left.\begin{aligned} \Theta_x &\equiv R_{tx} + n\left(u^{(0)}_x - u^{(0)}_{x(b)}\right),\\ \Theta_y &\equiv R_{ty} + \left(u^{(0)}_y - u^{(0)}_{y(b)}\right), \end{aligned}\right\} \tag{B3}$$

the integration of equations (B2) and (B3) together with the definitions of the strain rate components and the boundary conditions of equations (A8) and (A9) yields

$$\hat{\mathbf{u}}^{(1)} + \boldsymbol{\Lambda}\hat{\mathbf{u}}^{(1)}_{(s)} = \hat{\mathbf{u}}^{(\mathrm{S})(1)},$$

$$\boldsymbol{\Lambda} = \eta_{0(s)}\begin{bmatrix} \Theta_x\left(\frac{4}{n}k_x^2 + k_y^2\right) & \Theta_x k_x k_y\\ \Theta_y k_y k_x & \Theta_y\left(4k_y^2 + k_x^2\right)\end{bmatrix},$$

which yields this matrix equation for the surface velocities:

$$\left(\boldsymbol{\Lambda}_{(s)} + \mathbf{I}\right)\hat{\mathbf{u}}^{(1)}_{(s)} = \hat{\mathbf{u}}^{(\mathrm{S})(1)}_{(s)},$$

and this expression for the horizontal velocity vector:

$$\hat{\mathbf{u}}^{(1)} = \hat{\mathbf{u}}^{(\mathrm{S})(1)} - \boldsymbol{\Lambda}\left(\mathbf{I} + \boldsymbol{\Lambda}_{(s)}\right)^{-1}\hat{\mathbf{u}}^{(\mathrm{S})(1)}_{(s)}. \tag{B4}$$

The above is the corrected perturbed velocity using the $O(\delta)$ correction.

[55] A less accurate variant is to use the SIA to compute the surface velocity used in the longitudinal stress correction. This is given by the formula

$$\hat{\mathbf{u}}^{(\mathrm{L1S1})(1)} = \hat{\mathbf{u}}^{(\mathrm{S})(1)} - \boldsymbol{\Lambda}\left(\mathbf{I} - \boldsymbol{\Lambda}_{(s)}\right)\hat{\mathbf{u}}^{(\mathrm{S})(1)}_{(s)}. \tag{B5}$$

B2. L1L2, L1S2

[56] This uses a different expression for computing the longitudinal stresses. The mechanical equations are the same, but the invariant/viscosity approximations are somewhat different:

$$\left.\begin{aligned} \partial_\zeta\tau^{(0)}_{xz} &= -1, \qquad \tau^{(0)}_{jk} = Be^{(0)m}_{(s)}e^{(0)}_{jk},\\ \partial_\zeta u^{(0)}_j &= A\tau^{(0)n}\tau^{(0)}_{jz}, \quad \tau^{(0)2} = \tau^{(0)2}_s + \tau^{(0)2}_\ell. \end{aligned}\right\} \tag{B6}$$

The first-order momentum balance equations are equation (14), and the first-order shear relationships are

$$\left.\begin{aligned} \partial_\zeta\hat{u}^{(1)}_x &= C^{(0)}_{xzxz}\hat{\tau}^{(1)}_{xz} + C^{(0)}_{xzxx}\hat{\tau}^{(1)}_{xx} + \hat{H}^{(1)}\partial_\zeta u^{(0)}_x,\\ C^{(0)}_{xzxz} &= \tfrac{1}{\eta^{(0)}}\left(1 + (n-1)\tfrac{\tau^{(0)2}_{xz}}{\tau^{(0)2}}\right),\\ C^{(0)}_{xzxx} &= \tfrac{(n-1)}{\eta^{(0)}}\left(\tfrac{\tau^{(0)}_{xx}\tau^{(0)}_{xz}}{\tau^{(0)2}}\right),\\ \partial_\zeta\hat{u}^{(1)}_y &= \tfrac{1}{\eta^{(0)}}\hat{\tau}^{(1)}_{yz},\\ \upsilon\hat{e}^{(1)}_{xx(s)} &= C^{(0)}_{xxxx}\hat{\tau}^{(1)}_{xx} + C^{(0)}_{xxxz}\hat{\tau}^{(\mathrm{S})(1)}_{xz},\\ \hat{\tau}^{(\mathrm{S})(1)}_{xz} &= \tau^{(\mathrm{S})(0)}_{xz}\left(ik_x\hat{s}^{(1)} + H^{(1)}\right),\\ C^{(0)}_{xxxx} &= \tfrac{1}{2\eta^{(0)}}\left(1 + (n-1)\left(\tfrac{\tau^{(0)2}_{xx}}{\tau^{(0)2}}\right)\right),\\ C^{(0)}_{xxxz} &= \tfrac{(n-1)}{2\eta^{(0)}}\left(\tfrac{\tau^{(0)}_{xx}\tau^{(0)}_{xz}}{\tau^{(0)2}}\right). \end{aligned}\right\} \tag{B7}$$

Also, the following form is useful:

$$\left.\begin{aligned} \hat{\tau}^{(1)}_{xx} &= \tfrac{1}{C^{(0)}_{xxxx}}\upsilon\hat{e}^{(1)}_{xx(s)} - C^{(0)}_2\hat{\tau}^{(\mathrm{S})(1)}_{xz},\\ C^{(0)}_2 &= \tfrac{C^{(0)}_{xxxz}}{C^{(0)}_{xxxx}}. \end{aligned}\right\} \tag{B8}$$

The remaining statements of the constitutive relationships are

$$\left.\begin{aligned} \partial_\zeta \hat{u}_y^{(1)} &= \tfrac{1}{\eta^{(0)}}\hat{\tau}_{yz}^{(1)}, & \tfrac{1}{\eta^{(0)}} &= 2A\tau^{(0)(n-1)}, \\ \upsilon\hat{e}_{yy(s)}^{(1)} &= \tfrac{1}{2\eta^{(0)}}\hat{\tau}_{yy}^{(1)}, & \upsilon\hat{e}_{xy(s)}^{(1)} &= \tfrac{1}{2\eta^{(0)}}\hat{\tau}_{xy}^{(1)}. \end{aligned}\right\} \tag{B9}$$

Defining

$$\left.\begin{aligned} \psi_x &= 2ik_x\textstyle\int_\zeta^1 \frac{\upsilon \mathrm{d}\zeta'}{C_{xxxx}^{(0)}}, \\ \psi_z &= (1-\zeta) + 2ik_x\textstyle\int_\zeta^1 C_2^{(0)}(1-\zeta')\mathrm{d}\zeta', \\ \psi_H &= -ik_x\textstyle\int_\zeta^1 \partial_\zeta\tau_{xx}^{(0)}\zeta'\mathrm{d}\zeta', \\ \psi_b &= -ik_x\left(\tau_{xx(s)}^{(0)} - \tau_{xx}^{(0)}\right), \psi_y = 2\textstyle\int_\zeta^1 \upsilon\eta^{(0)}\mathrm{d}\zeta', \\ F_x &= \textstyle\int_0^\zeta \left(C_{xzxz}^{(0)}\psi_x - \frac{C_{xzxx}^{(0)}}{C_{xxxx}^{(0)}}\right)\mathrm{d}\zeta' + R_{tx}\psi_{x(b)}, \\ F_z &= \textstyle\int_0^\zeta \left(C_{xzxz}^{(0)}\psi_z - C_{xzxx}^{(0)}C_2^{(0)}\right)\mathrm{d}\zeta' + R_{tx}\psi_{z(b)}, \\ F_y &= \textstyle\int_0^\zeta C_{xzxz}^{(0)}\psi_y\mathrm{d}\zeta' + R_{tx}\psi_{y(b)}, \\ F_H &= \textstyle\int_0^\zeta C_{xzxz}^{(0)}\psi_H\mathrm{d}\zeta' + R_{tx}\psi_{H(b)}, \\ F_b &= \textstyle\int_0^\zeta C_{xzxz}^{(0)}\psi_b\mathrm{d}\zeta' + R_{tx}\psi_{b(b)}, \end{aligned}\right\} \tag{B10}$$

integration of equations (14) and (B7) and the boundary conditions of equations (A8) and (A9) yields

$$u_x^{(1)} + \hat{e}_{xx(s)}^{(1)}F_x + ik_y\hat{e}_{xy(s)}^{(1)}F_y = F_z\hat{\tau}_{xz(b)}^{(\mathrm{S})(1)} + F_H\hat{H}^{(1)} + F_b\hat{b}^{(1)} + \hat{H}^{(1)}\left(u^{(0)} - u_{(b)}^{(0)}\right). \tag{B11}$$

The solution for the transverse component of the horizontal velocity is given by

$$\left.\begin{aligned} G_x &= \textstyle\int_0^\zeta \frac{1}{\eta^{(0)}}\psi_y\mathrm{d}\zeta' + R_{ty}\psi_{y(b)}, \\ G_y &= 2\textstyle\int_0^\zeta \frac{1}{\eta^{(0)}}\psi_y\mathrm{d}\zeta' + 2R_{ty}\psi_{y(b)}, \\ \hat{u}_y^{(1)} &= -\left(k_y^2G_y + \tfrac{1}{2}k_x^2G_x\right)\hat{u}_{y(s)}^{(1)} - \tfrac{1}{2}k_yk_xG_x\hat{u}_{x(s)}^{(1)} + \hat{u}_y^{(\mathrm{SQU})(1)}, \end{aligned}\right\} \tag{B12}$$

and the following equation for the velocity field emerges:

$$\hat{\mathbf{u}}^{(1)} + \mathbf{\Gamma}\hat{\mathbf{u}}_{(s)}^{(1)} = \mathbf{r}, \tag{B13}$$

where

$$\mathbf{r} = \begin{bmatrix} F_z\hat{\tau}_{xz(b)}^{(\mathrm{S})(1)} + F_H\hat{H}^{(1)} + \hat{H}^{(1)}\left(u_{x(s)}^{(0)} - u_{x(b)}^{(0)}\right) \\ \hat{u}_{y(s)}^{(\mathrm{SQU})(1)} \end{bmatrix}, \tag{B14}$$

$$\mathbf{\Gamma} = \begin{bmatrix} \left(-ik_xF_x + \tfrac{1}{2}k_y^2F_y\right) & \tfrac{1}{2}k_xk_yF_y \\ \tfrac{1}{2}k_xk_yG_x & \left(k_y^2G_y + \tfrac{1}{2}k_x^2G_x\right) \end{bmatrix}. \tag{B15}$$

In addition, the surface velocities may be computed to give the complete velocity field:

$$\mathbf{u}_{(s)}^{(1)} = \left(\mathbf{I} + \mathbf{\Gamma}_{(s)}\right)^{-1}\mathbf{r}_{(s)} \tag{B16}$$

$$\mathbf{u}^{(1)} = \mathbf{r} - \mathbf{\Gamma}\left(\mathbf{I} + \mathbf{\Gamma}_{(s)}\right)^{-1}\mathbf{r}_{(s)} \tag{B17}$$

if we use the SIA mechanics and shear relationship for the surface velocity, $u_{(s)}^{(\mathrm{S})(1)}$, which can be substituted for the surface velocity in equation (B13) to get

$$\hat{\mathbf{u}}^{(1)} = \mathbf{r} - \mathbf{\Gamma}\hat{\mathbf{u}}_{(s)}^{(S)(1)}. \tag{B18}$$

This turns out to be unstable, at least some of the time.

Appendix C: Analytical Solution for LMLa

[57] When the rheology is Newtonian, the model LMLa, defined by equations (14), (15), and (20), can be perturbed about the zeroth-order solution (equation (33)) to yield some first-order equations. In this Appendix an analytical solution of these equations for the case of plane flow is presented. The procedure of *Gudmundsson* [2003] is followed, and a transformed coordinate system is not used. Thus, instead of equation (25), one has

$$\left.\begin{aligned} H^{(1)} &= \Re\left\{\hat{H}^{(1)}\exp(\lambda t - i\mathbf{k}\cdot\mathbf{r})\right\}, \\ \mathbf{v}^{(1)} &= \Re\left\{\hat{\mathbf{v}}^{(1)}(z)\exp(\lambda t - i\mathbf{k}\cdot\mathbf{r})\right\}. \end{aligned}\right\} \tag{C1}$$

[58] The scaling is specified such that in the zeroth-order flow the base and upper surface are at $z = 0$ and $z = 1$, respectively. This means that the derivatives with respect to ζ in equation (33) are numerically equal to derivatives with respect to z (for the zeroth-order equations only). The first-order boundary conditions are applied at $z = b^{(1)}$ and $z = s^{(1)}$, respectively. The field equations are

$$\left.\begin{aligned} \partial_z\tau_{xz}^{(1)} + \partial_x\tau_{xx}^{(1)} &= \partial_xp^{(1)}, & -\partial_z\tau_{xx}^{(1)} &= \partial_zp^{(1)}, \\ e_{xz}^{(1)} &= \tfrac{1}{2}\partial_zu^{(1)}, & e_{xx}^{(1)} &= \partial_xu^{(1)}, \\ \tau_{xz}^{(1)} &= \eta\partial_zu^{(1)}, & \tau_{xx}^{(1)} &= 2\eta\partial_xu^{(1)} \end{aligned}\right\} \tag{C2}$$

applied in $b^{(1)} \le z \le s^{(1)}$, and therefore

$$\eta\partial_z^2u^{(1)} + 2\eta\partial_x^2u^{(1)} = \partial_xp^{(1)}, \qquad -2\eta\partial_x\partial_zu^{(1)} = \partial_zp^{(1)}, \tag{C3}$$

which in Fourier space can be written

$$\eta\mathrm{d}_z^2\hat{u}^{(1)} - 2k_x^2\eta\hat{u}^{(1)} = -ik_x\hat{p}^{(1)}, \qquad 2ik_x\eta\mathrm{d}_z\hat{u}^{(1)} = \mathrm{d}_z\hat{p}^{(1)}, \tag{C4}$$

which has solution

$$\left.\begin{aligned} \hat{u}^{(1)} &= U_1\exp(-2k_xz) + U_2\exp(2k_xz) + U_3, \\ \hat{p}^{(1)} &= 2ik_x\eta(U_1\exp(-2k_xz) + U_2\exp(2k_xz) - U_3), \\ \hat{w}^{(1)} &= -\tfrac{i}{2}U_1\exp(-2k_xz) + \tfrac{i}{2}U_2\exp(2k_xz) + iU_3z + W_1, \end{aligned}\right\} \tag{C5}$$

where the constants U_1, U_2, U_3, and W_1 are given by the boundary conditions. The first-order Fourier-transformed boundary conditions evaluated at $s^{(1)}$ and $b^{(1)}$, corresponding to equations (A8) and (A9), are

$$\left.\begin{aligned}
\hat{\tau}^{(1)}_{xz(s)} + s^{(1)}\partial_z \tau^{(0)}_{xz(s)} &= 0,\\
\hat{\sigma}^{(1)}_{zz(s)} &= s^{(1)}\partial_z p^{(0)}_{(s)},\\
\hat{T}^{(1)}_{tx(b)} &= \hat{\tau}^{(1)}_{xz(b)} + b^{(1)}\partial_z \tau^{(0)}_{xz(b)},\\
\hat{T}^{(1)}_{n(b)} &= \hat{\sigma}^{(1)}_{zz(b)} - b^{(1)}\partial_z p^{(0)}_{(b)},\\
\hat{u}^{(1)}_{(b)} + b^{(1)}\partial_z u^{(0)}_{(b)} &= R_t \hat{T}^{(1)}_{tx(b)} + R_n \hat{T}^{(1)}_{n(b)},\\
\hat{w}^{(1)}_{(b)} &= -\mathrm{i}\hat{b}^{(1)} u^{(0)}_{(b)} k_x.
\end{aligned}\right\} \qquad \text{(C6)}$$

Substitution of the solutions of equation (C5) into equation (C6) yields four linear equations in U_1, U_2, U_3, and W_1. The solutions are rather lengthy and consequently are not presented here, but they are readily obtainable using computer algebra software.

[59] **Acknowledgments.** Thanks to Hilmar Gueth Mundsson for many discussions and to the referees and editors for identifying and clarifying many ambiguities.

References

Baral, D. R., K. Hutter, and R. Greve (2001), Asymptotic theories of large-scale motion, temperature and moisture distribution in land-based polythermal ice sheets: A critical review and new developments, *Appl. Mech. Rev.*, *54*(3), 215–256.

Blatter, H. (1995), Velocity and stress-fields in grounded glaciers—A simple algorithm for including deviatoric stress gradients, *J. Glaciol.*, *41*(138), 333–344.

Budd, W. F. (1970), The longitudinal stress and strain-rate gradients in ice masses, *J. Glaciol.*, *9*(55), 19–27.

Collins, I. F. (1968), On the use of the equilibrium equations and flow law in relating the surface and bed topography of glaciers and ice sheets, *J. Glaciol.*, *7*(50), 199–204.

Dahl-Jensen, D. (1989), Steady thermomechanical flow along two-dimensional flow lines in large grounded ice sheets, *J. Geophys. Res.*, *94*(B8), 10,355–10,362.

Fornberg, B. (1996), *A Practical Guide to Pseudospectral Methods*, Cambridge Univ. Press, New York.

Gudmundsson, G. H. (2003), Transmission of basal variability to a glacier surface, *J. Geophys. Res.*, *108*(B5), 2253, doi:10.1029/2002JB002107.

Hindmarsh, R. C. A. (1993), Qualitative dynamics of marine ice sheets, in *Ice in the Climate System*, *NATO ASI Ser. I*, vol. 12, *Global Environmental Change*, edited by W. R. Peltier, pp. 67–99, Springer-Verlag, New York.

Hindmarsh, R. C. A. (1998), The stability of a viscous till sheet coupled with ice flow, considered at wavelengths less than the ice thickness, *J. Glaciol.*, *44*(147), 285–292.

Hindmarsh, R. C. A. (1999), On the numerical computation of temperature in an ice-sheet, *J. Glaciol.*, *45*(151), 568–574.

Hindmarsh, R. C. A., and K. Hutter (1988), Numerical fixed domain mapping solution of free surface flows coupled with an evolving interior field, *Int. J. Numer. Anal. Methods Geomech.*, *12*, 437–459.

Hubbard, A. L., H. Blatter, P. W. Nienow, D. Mair, and B. Hubbard (1998), Comparison of a three-dimensional model for glacier flow with field data from Haut Glacier d'Arolla, Switzerland, *J. Glaciol.*, *44*(147), 368–378.

Hutter, K. (1983), *Theoretical Glaciology*, D. Riedel, Norwell, Mass.

Huybrechts, P. (1992), The Antarctic ice sheet and environmental change: A three-dimensional modelling study, *Ber. Polarforsch.*, *99*, 1–241.

Johannesson, T. (1992), The landscape of temperate ice caps, Ph.D. thesis, Univ. of Wash., Seattle.

Kamb, B., and K. A. Echelmeyer (1986), Stress-gradient coupling in glacier flow: I. Longitudinal averaging of the influence of ice thickness and surface slope, *J. Glaciol.*, *32*(111), 267–284.

Leysinger Vieli, G. J.-M. C., and G. H. Gudmundsson (2004), On estimating length fluctuations of glaciers caused by changes in climatic forcing, *J. Geophys. Res.*, *109*, F01007, doi:10.1029/2003JF000027.

MacAyeal, D. R. (1989), Large-scale ice flow over a viscous basal sediment: Theory and application to Ice Stream B, Antarctica, *J. Geophys. Res.*, *94*(B4), 4071–4087.

Morland, L. W. (1984), Thermo-mechanical balances for ice sheets, *Geophys. Astrophys. Fluid Dyn.*, *29*, 237–266.

Muszynski, I., and G. E. Birchfield (1987), A coupled marine ice-stream-ice-shelf model, *J. Glaciol.*, *33*(113), 3–15.

Nye, J. F. (1959), The motion of ice sheets and glaciers, *J. Glaciol.*, *3*(26), 493–507.

Nye, J. F. (1969), The effect of longitudinal stress on the shear stress at the base of an ice sheet, *J. Glaciol.*, *8*(53), 207–213.

Pattyn, F. (2003), A new three-dimensional higher-order thermomechanical ice sheet model: Basic sensitivity, ice stream development, and ice flow across subglacial lakes, *J. Geophys. Res.*, *108*(B8), 2382, doi:10.1029/2002JB002329.

Ritz, C., V. Rommelaere, and C. Dumas (2001), Modeling the evolution of Antarctic ice sheet over the last 420,000 years: Implications for altitude changes in the Vostok region, *J. Geophys. Res.*, *106*(D23), 31,943–31,964.

Robin, G. Q. (1967), Surface topography of ice sheets, *Nature*, *215*(5105), 1–20.

Saito, F., A. Abe-Ouchi, and H. Blatter (2004), Effects of the first-order stress gradients to an ice sheet evaluated by a three-dimensional thermomechanical coupled model, *Ann. Glaciol.*, *37*, 166–172.

Trefethen, L. N. (2000), *Spectral Methods in Matlab*, Soc. for Ind. and Appl. Math., Philadelphia, Pa.

Van der Veen, C. J., and I. Whillans (1989), Force budget: I. Theory and numerical methods, *J. Glaciol.*, *35*(119), 53–60.

Wilchinsky, A. V., and V. A. Chugonov (2000), Ice-stream-ice-shelf transition: Theoretical analysis of two-dimensional flow, *Ann. Glaciol.*, *30*, 153–162.

R. C. A. Hindmarsh, Physical Science Division, British Antarctic Survey, Natural Environment Research Council, High Cross, Madingley Road, Cambridge, CB3 0ET, UK. (rcah@bas.ac.uk)